Table 1
Effect of maternal *Sirt3* genotype on IVF rate

Genotype		IVF (*n*)		Fertilization rate
Sperm	Egg	Fertilized	Unfertilized	
Sirt3$^+$	*Sirt3*$^+$	51	19	73%
Sirt3$^+$	*Sirt3*$^-$	62	28	69%
Sirt3$^-$	*Sirt3*$^+$	62	10	86%
Sirt3$^-$	*Sirt3*$^-$	65	31	68%

Cochran-Mantel-Haenszel χ^2 test stratified on sperm genotype.
$\chi^2 = 4.701$; $P = 0.030$; odds ratio 1.813.

down embryos (our unpublished observations), which indicates that Foxo3a might not be contributing to the protective role of Sirt3 against oxidative stress in preimplantation embryos.

Involvement of p53 in ROS-induced preimplantation developmental arrest in Sirt3-deficient embryos. Mitochondrial ROS increase in Sirt3-knockdown embryos is accompanied by upregulation of p53 expression. Furthermore, siRNA-induced p53 knockdown improved developmental outcome in Sirt3-knockdown embryos.

Under normal conditions, levels of p53 protein are kept low because of its short half-life through the ubiquitin-proteasome degradation pathway, mediated by E3 ubiquitin ligase Mdm2, in preimplantation embryos as well as in various somatic cells (35, 46). Upon stress conditions, modification (e.g., phosphorylation) of p53 and/or Mdm2 causes p53 stabilization and activation by inhibiting the p53-Mdm2 interaction (35). In in vitro–cultured preimplantation embryos, the latency of p53 is maintained by the phosphatidylinositol-3′-kinase/Akt–mediated activation of Mdm2 (46). Perturbation of this pathway, as well as Mdm2 inactivation, results in the accumulation of p53 and developmental arrest (46–48), which indicates that the latency of p53 is important for normal preimplantation development. Although mitochondrial ROS has proved to contribute to stress-induced p53 activation in some somatic cells (49), the involvement of p53 in the stress response of preimplantation embryos has been controversial (50, 51). The present study indicated that p53 is involved in developmental arrest induced by mitochondrial ROS in Sirt3-knockdown embryos.

Sirt3-related mechanisms independent of ROS may be involved in p53 activation in cooperation with mitochondrial ROS. AMPK, which responds to an increase in AMP/ATP ratio during calorie restriction, can activate p53 by increasing transcription of *p53* and through direct phosphorylation of p53 (52, 53). This pathway might be activated in Sirt3-deficient embryos, in which mitochondrial ATP synthesis is possibly decreased (30). Another possibility is that Sirt3 may deacetylate p53 as well as Sirt1 (54, 55), and, in the absence of Sirt3, acetylated p53 may accumulate in embryos. p53 acetylation is induced in response to stress and causes its activation and stabilization (54–56). Furthermore, p53 has recently been reported to localize to mitochondria (57). Thus, it would be interesting to test whether acetylated p53 could serve as a substrate for Sirt3 deacetylase activity.

The present study showed that expression of *Nanog* was downregulated in Sirt3-knockdown or -knockout embryos, and expression of *p21* was upregulated. Although it may simply reflect developmental delay, this finding is compatible with previous reports that p53 suppresses *Nanog* expression in ES cells after DNA damage, which may serve as a mechanism to maintain genomic stability in ES cells (39, 40). We speculate that, in the absence of Sirt3, p53 is activated by excessive mitochondrial ROS to prevent the generation of embryos carrying serious mutations partly through changes in p21 and Nanog activity.

Conclusion. We have identified Sirt3 as a protective factor against stress in preimplantation development under IVF and in vitro culture conditions. Sirt3 deficiency caused increased mitochondrial ROS production and subsequent developmental arrest attributed to p53 activation in preimplantation embryos. The present findings may contribute to the understanding of preimplantation biology and give a clue to the better outcome of assisted reproductive technologies.

Methods

Mice. ICR mice from Charles River Laboratories Japan Inc. were used in all experiments, except for those using C57BL6-background Sirt3-knockout mice with the *Sirt3*$^{Gt(neo)218Lex}$ allele (here referred to as *Sirt3*$^-$), which were generated by Lexicon Genetics and obtained from Mutant Mouse Regional Resource Centers. Mice were housed in an environmentally controlled room at 23°C ± 2°C, with 50%–60% relative humidity, under a 12-hour light/12-hour dark cycle. All animal experiments were approved by the Animal Care and Use Committee of the University of Tokyo and were performed in accordance with institutional guidelines.

Collection of eggs, IVF, and assessment of in vitro development. Female mice (8–10 weeks old) were superovulated with intraperitoneal injections of 7.5 IU pregnant mare serum gonadotropin (PMSG; Teikoku Hormone Mfg.) and, 48 hours later, 7.5 IU human chorionic gonadotropin (hCG; Teikoku Hormone Mfg.). Eggs were recovered from the oviducts 20 hours after hCG injection, and cumulus cells were extensively dispersed with 1 mg/ml hyaluronidase (Sigma-Aldrich). Sperm were expelled from the cauda epididymis of male mice into 200 μl human tubal fluid (HTF) medium and incubated under mineral oil for 1–2 hours at 37°C to capacitate. A sperm suspension at a concentration of 6–7 × 10^5 sperm/ml was used to inseminate eggs in a 200-μl drop of HTF medium under mineral oil. After coincubation with sperm for 6 hours, the inseminated eggs were washed and cultured in 50-μl droplets of potassium simplex optimized medium (KSOM; Specialty Media) under mineral oil at 37°C in humidified air containing 5% CO_2. Experiments at low oxygen concentration were performed in a humidified airtight chamber maintained at 37°C and flushed with a mixture of 5% O_2 and 5% CO_2 balanced with N_2. In experiments with inhibitors, each medium was supplemented with 5 mM nicotinamide (Sigma-Aldrich), 200 μM sirtinol (Calbiochem), 2 μM BML-210 (Biomol), 500 μM NAC (Wako), or DMSO (Sigma-Aldrich) alone. Cleavage and embryo development were examined every 24 hours.

Table 2
Effect of maternal *Sirt3* genotype on blastocyst formation rate after IVF

Genotype		Blastocysts (*n*)		Formation rate
Sperm	Egg	Formed	Unformed	
Sirt3$^+$	*Sirt3*$^+$	30	1	97%
Sirt3$^+$	*Sirt3*$^-$	19	13	59%
Sirt3$^-$	*Sirt3*$^+$	39	3	93%
Sirt3$^-$	*Sirt3*$^-$	30	15	67%

Cochran-Mantel-Haenszel χ^2 test stratified on sperm genotype.
$\chi^2 = 19.263$; $P < 0.001$; odds ratio 9.666.

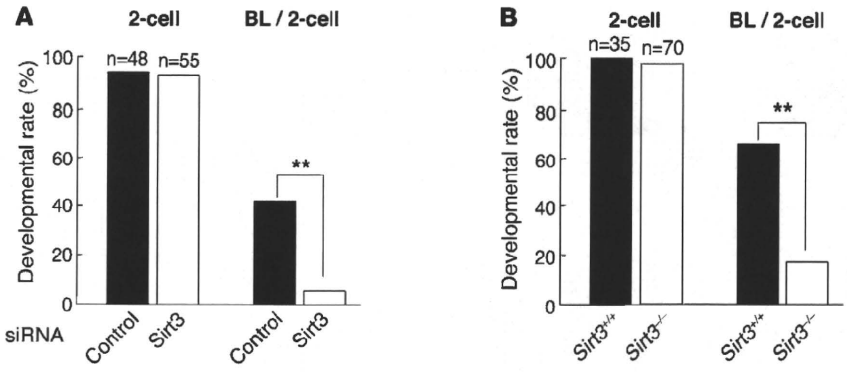

Figure 8

Parthenogenetic development is blocked by Sirt3 deficiency. (**A**) After Sr^{2+} activation for 4.5 hours, eggs that formed 2 pronuclei were injected with control or Sirt3 siRNA, and the rates of 2-cell and blastocyst formation were evaluated. (**B**) Eggs collected from wild-type and *Sirt3*$^{-/-}$ female mice underwent parthenogenetic activation. Data are derived from 4 (**A**) or 2 (**B**) independent experiments. Statistical assessments were performed by applying Fisher's exact test. $^{**}P < 0.001$.

Assessment of in utero development. Female ICR mice (8–10 weeks old) were bred with vasectomized ICR males to stimulate pseudopregnancy. Vaginal plug–positive females were used as recipients. Cultured embryos were transferred to recipients on day 0.5 of pseudopregnancy according to standard procedures. 7–10 embryos were transferred into each fallopian tube. Recipients were subjected to cesarean section on day 18.5 to determine the developmental competence of transferred embryos.

Parthenogenetic activation of eggs. ICR mouse eggs were activated by a 3- to 4-hour treatment with 10 mM Sr^{2+} prepared in Ca^{2+}-free M16 medium. Cytochalasin B (Sigma-Aldrich), an inhibitor of actin filament polymerization, was used to suppress the second polar body extrusion to generate diploid parthenotes. Activated eggs with 2 pronuclei, visualized under a differential interference contrast microscope, were defined as diploid parthenotes. Activated eggs were washed extensively and cultured in vitro under the same conditions as were IVF zygotes.

Plasmids. Mouse *Sirt1*, *Sirt2*, and *Sirt3* cDNAs were cloned by RT-PCR on total RNA from NIH 3T3 cells. For EGFP fusion constructs, cDNA fragments encompassing the open reading frame of *Sirt1*, *Sirt2*, and *Sirt3* were subcloned in frame into the pEGFP-N3 expression vector (Clontech). The fragments encoding the fusion constructs were then subcloned into pCRII-TOPO (Invitrogen) for in vitro transcription. The constructs were verified by sequencing.

Cell culture and transfection. NIH 3T3 cells were cultured in Dulbecco modified Eagle medium containing 10% fetal calf serum and antibiotics at 37°C in 5% CO_2. For siRNA transfection, cells were grown to 30%–50% confluence and treated with a mixture of siRNA and oligofectamine reagents (Invitrogen) according to the manufacturer's protocol.

Conventional RT-PCR. Female ICR mice (8–10 weeks old) were superovulated as above and used for collection of eggs or mated with ICR male mice to obtain early embryos at different stages. In some experiments, in vitro–cultured embryos and NIH 3T3 cells were collected at the indicated times. Samples were lysed in lysing buffer (Isogen; Nippon Gene), with volumes adjusted according to the number of eggs or embryos, and subjected to RNA extraction according to standard procedures. After reverse transcription with Quantiscript Reverse Transcriptase and RT Primer Mix (QuantiTect Reverse Transcription; Qiagen), PCR amplification was performed using specific primers listed in Supplemental Table 1. Thermal cycling was performed for 30–35 cycles

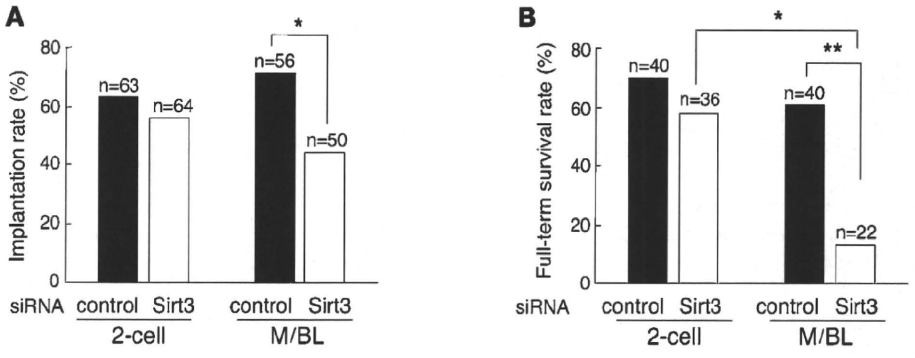

Figure 9

Long-term in vitro culture leads to decreased implantation and full-term survival rates in Sirt3-knockdown embryos. (**A** and **B**) Implantation rates (**A**) and full-term survival rates (**B**) of embryos injected with Sirt3 or control siRNA and transferred into pseudopregnant mice at the 2-cell or morula/blastocyst stage. Implantation sites and viability of fetuses were inspected by cesarean section 18 days after transfer. Implantation rate was estimated by the number of implantation sites; full-term survival rate was assessed by dividing the number of live pups by the number of implantation sites. Data are derived from 5 (2-cell embryo transfer) or 4 (morula/blastocyst transfer) independent experiments. Statistical assessments were performed by applying Ryan's multiple-comparison test. $^{*}P < 0.005$; $^{**}P < 0.001$.

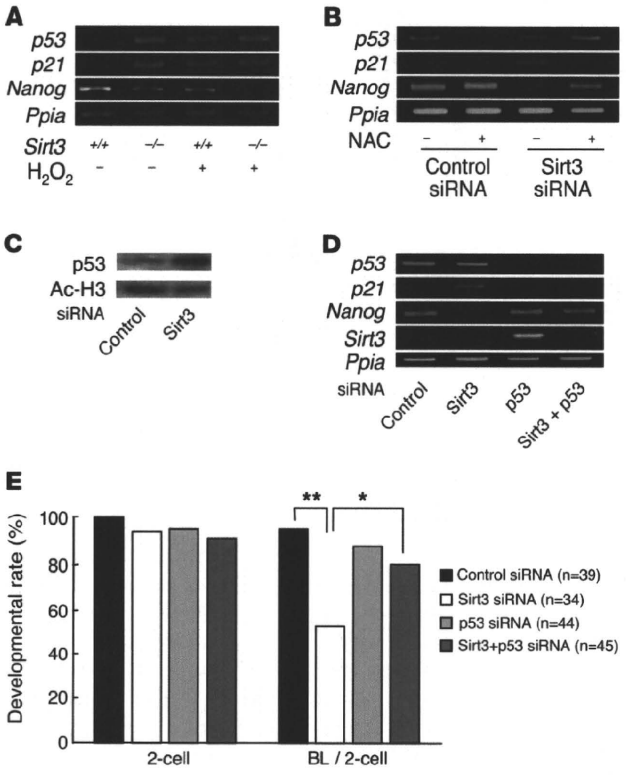

Figure 10

Involvement of p53 in developmental arrest of Sirt3-deficient preimplantation embryos. (**A**) *p53* and *p21* were upregulated in *Sirt3*$^{-/-}$ embryos as in H_2O_2-treated wild-type embryos. *Nanog* expression was decreased in *Sirt3*$^{-/-}$ embryos, and the decrease was enhanced by H_2O_2 stimulus. (**B**) Effects of Sirt3 knockdown and treatment with NAC on the expression of *p53* and its downstream genes. In Sirt3 siRNA–injected embryos, *p21* expression was upregulated, whereas *Nanog* expression was downregulated. These effects were blocked by NAC. (**C**) Western blotting analysis showing increased p53 protein levels in Sirt3-knockdown embryos at the morula stage. Signals for acetylated histone H3 (Ac-H3) served as an internal control. (**D**) Effects of p53 knockdown on Sirt3 siRNA–induced changes in the expression of genes downstream of p53. Sirt3 siRNA–induced *p21* upregulation and *Nanog* downregulation were blocked by siRNA-mediated p53 knockdown. *Ppia* expression served as an internal control in **A**, **B**, and **D**. (**E**) Effects of p53 knockdown on preimplantation developmental arrest in Sirt3-knockdown embryos. The rate of blastocyst formation was significantly improved by coinjection with p53 siRNA. Data are derived from 4 independent experiments. Statistical assessments were performed by applying Ryan's multiple-comparison test. *$P < 0.05$; **$P < 0.001$.

to maintain PCR conditions within the linear range of amplification before saturation was reached. Each cycle consisted of 30 seconds of denaturation at 94°C, 30 seconds of annealing at each annealing temperature (Supplemental Table 1), and 30 seconds of extension at 72°C. Signals for *Gapdh* and peptidylprolyl isomerase A (*Ppia*) expression served as internal controls.

Quantitative real-time PCR. Quantification of each mRNA level was performed by real-time RT-PCR analyses using a LightCycler (Roche) and Real-Time PCR Premix with SYBR Green (RBC Bioscience) following the manufacturers' protocols. Each cycle consisted of 10 seconds of denaturation at 94°C, 13–15 seconds of annealing at each annealing temperature (Supplemental Table 2), and 12–13 seconds of extension at 72°C. Thermal cycling was performed for 45–50 cycles. The second-derivative maximum method was adopted to determine the crossing points automatically for individual samples, and relative amounts of mRNA were calculated based on the crossing-point analysis. *Ppia* was used as an internal control. The result was expressed as fold change relative to control.

Western blotting. A pool of approximately 50 early embryos or NIH 3T3 cells was lysed in Laemmli buffer containing protease inhibitors, and then subjected to 12% SDS-PAGE. The separated proteins were transferred to a nylon membrane, which was then pretreated with 3% bovine serum albumin for blocking and incubated with primary antibodies as follows: rabbit anti-Sirt3 antibody (Abgent) for NIH 3T3 cell samples, rabbit anti-Sirt3 antibody from E. Verdin (UCSF, San Francisco, California, USA; ref. 26) for early embryo samples, and mouse anti-p53 antibody (BD Biosciences – Pharmingen). Blots were then incubated with anti-rabbit or anti-mouse IgG antibody conjugated to horseradish peroxidase (ICN). The protein bands were visualized using an ECL Plus Western Blotting Detection System (Amersham Pharmacia Biotech). The membrane was then washed and reblotted with anti-α-tubulin antibody (Sigma-Aldrich) or anti-acetylated histone H3 antibody (Cell Signaling Technology) for an internal control. Densitometric quantification was performed with ImageJ software (NIH).

RNAi. Chemically synthesized 25-nucleotide stealth RNAi duplex oligonucleotides were commercially obtained (Invitrogen). We selected 2 different sequences for each of the genes, *Sirt3* and *p53*, selected for the generation of siRNA: the sequences for siRNAs 1 and 2 corresponded, respectively, to nucleotides 355–379 and 386–410 of mouse *Sirt3* (GenBank accession no. NM_022433) and to nucleotides 985–1,009 and 165–189 of mouse *p53* (GenBank accession no. NM_011640; Supplemental Table 2). Stealth RNAi negative control HiGC (Invitrogen) was used as control siRNA. Approximately 10 pl of 20 μM siRNA was injected into the cytoplasm of fertilized eggs. The efficiency of gene knockdown was evaluated by RT-PCR with primers specific for mouse *Sirt3* and *p53* mRNA (Supplemental Table 1).

In vitro transcription and RNA microinjection. Preparation and injection of in vitro–transcribed mRNA were performed as previously described (58). Briefly, plasmids containing Sirt1-EGFP, Sirt2-EGFP, and Sirt3-EGFP fusion constructs and EGFP alone were linearized and used as templates for in vitro transcription using the T7 MessageMachine kit (Ambion). Synthesized RNA was further polyadenylated by yeast poly(A) polymerase (Amersham Biosciences) and resolved in 150 mM KCl with a final concentration of approximately 100 ng/μl. The diluted RNA was filtered, heated at 90°C for 1 minute, and cooled on ice. Then, approximately 10 pl RNA solution was injected into fertilized eggs through a glass micropipette. Embryos were grown to the 2-cell stage, at which time confocal images were obtained using a Nikon D-ECLIPSE C1 system.

Detection of intracellular ROS. To detect intercellular ROS in living embryos, we used CM-H_2DCFDA from Invitrogen. CM-H_2DCFDA was prepared in DMSO immediately prior to loading. Embryos were incubated with 10 μM CM-H_2DCFDA for 30 minutes and observed under a laser scanning confocal microscope (Nikon D-ECLIPSE C1), with an excitation wavelength of

480 nm and an emission wavelength of 505–530 nm. In some experiments, embryos were pretreated with the NAD(P)H oxidase inhibitor apocynin (100 μM) or the ubiquinol/cytochrome *c* oxidoreductase inhibitor stigmatellin (10 μM) for 30 minutes.

Statistics. Differences between 2 groups were analyzed by Mann-Whitney *U* test. Multiple comparisons between more than 2 groups were analyzed by 1-way ANOVA and post-hoc tests as indicated in the figure legends. Continuous data are presented as mean ± SEM. *P* values less than 0.05 were considered significant.

Acknowledgments

We thank Eric Verdin for Sirt3 antibody; Atsuo Ogura, Hiroshi Suzuki, and Kiyoshi Kita for helpful discussions and comments; Yuko Fujisawa for technical assistance; and Chisato Fujimoto for statistical analysis. This work was supported in part by Global COE Program (Integrative Life Science Based on the Study of Biosignaling Mechanisms); MEXT, Japan; grants-in-aid for scientific research from the Ministry of Education, Culture, Sports, Science and Technology of Japan; and grants-in-aid for scientific research from the Ministry of Health, Labor, and Welfare of Japan.

Received for publication December 14, 2009, and accepted in revised form June 9, 2010.

Address correspondence to: Hiroki Kurihara, Department of Physiological Chemistry and Metabolism, Graduate School of Medicine, University of Tokyo, 7-3-1 Hongo, Bunkyo-ku, Tokyo 113-0033, Japan. Phone: 81.3.5841.3498; Fax: 81.3.5684.4958; E-mail: kuri-tky@umin.ac.jp.

Nanao Horike's present address is: Animal Models of Human Diseases, National Institute of Biomedical Innovation, Osaka, Japan.

Tomokazu Amano's present address is: Developmental Genomics and Aging Section, Laboratory of Genetics, National Institute on Aging, NIH, Baltimore, Maryland, USA.

1. Matzuk MM, Lamb DJ. The biology of infertility: research advances and clinical challenges. *Nat Med.* 2008;14(11):1197–1213.
2. Smith S, Pfeifer SM, Collins JA. Diagnosis and management of female infertility. *JAMA.* 2003; 290(13):1767–1770.
3. Van Voorhis BJ. Clinical practice. In vitro fertilization. *N Engl J Med.* 2007;356(4):379–386.
4. Baird DD, Wilcox AJ, Weinberg CR. Use of time to pregnancy to study environmental exposures. *Am J Epidemiol.* 1986;124(3):470–480.
5. Witschi E. Natural control of fertility. *Fertil Steril.* 1968;19(1):1–14.
6. Van Blerkom J. Mitochondria in early mammalian development. *Semin Cell Dev Biol.* 2009; 20(3):354–364.
7. Wilding M, Coppola G, Dale B, Di Matteo L. Mitochondria and human preimplantation embryo development. *Reproduction.* 2009;137(4):619–624.
8. Thompson JG, McNaughton C, Gasparrini B, McGowan LT, Tervit HR. Effect of inhibitors and uncouplers of oxidative phosphorylation during compaction and blastulation of bovine embryos cultured in vitro. *J Reprod Fertil.* 2000;118(1):47–55.
9. Thouas GA, Trounson AO, Wolvetang EJ, Jones GM. Mitochondrial dysfunction in mouse oocytes results in preimplantation embryo arrest in vitro. *Biol Reprod.* 2004;71(6):1936–1942.
10. Trimarchi JR, Liu L, Porterfield DM, Smith PJ, Keefe DL. Oxidative phosphorylation-dependent and -independent oxygen consumption by individual preimplantation mouse embryos. *Biol Reprod.* 2000;62(6):1866–1874.
11. Van Blerkom J, Davis PW, Lee J. ATP content of human oocytes and developmental potential and outcome after in-vitro fertilization and embryo transfer. *Hum Reprod.* 1995;10(2):415–424.
12. Raha S, Robinson BH. Mitochondria, oxygen free radicals, disease and ageing. *Trends Biochem Sci.* 2000;25(10):502–508.
13. Zhang DX, Gutterman DD. Mitochondrial reactive oxygen species-mediated signaling in endothelial cells. *Am J Physiol Heart Circ Physiol.* 2007; 292(5):H2023–H2031.
14. Brookes PS, Yoon Y, Robotham JL, Anders MW, Sheu SS. Calcium, ATP, and ROS: a mitochondrial love-hate triangle. *Am J Physiol Cell Physiol.* 2004;287(4):C817–C833.
15. Covarrubias L, Hernandez-Garcia D, Schnabel D, Salas-Vidal E, Castro-Obregon S. Function of reactive oxygen species during animal development: passive or active? *Dev Biol.* 2008;320(1):1–11.
16. Ruder EH, Hartman TJ, Blumberg J, Goldman MB. Oxidative stress and antioxidants: exposure and impact on female fertility. *Hum Reprod Update.* 2008;14(4):345–357.
17. Agarwal A, Gupta S, Sekhon L, Shah R. Redox considerations in female reproductive function and assisted reproduction: from molecular mechanisms to health implications. *Antioxid Redox Signal.* 2008;10(8):1375–1403.
18. Liu L, Trimarchi JR, Keefe DL. Involvement of mitochondria in oxidative stress-induced cell death in mouse zygotes. *Biol Reprod.* 2000;62(6):1745–1753.
19. Finkel T, Deng CX, Mostoslavsky R. Recent progress in the biology and physiology of sirtuins. *Nature.* 2009;460(7255):587–591.
20. Schwer B, Verdin E. Conserved metabolic regulatory functions of sirtuins. *Cell Metab.* 2008;7(2):104–112.
21. Longo VD, Kennedy BK. Sirtuins in aging and age-related disease. *Cell.* 2006;126(2):257–268.
22. Imai S, Armstrong CM, Kaeberlein M, Guarente L. Transcriptional silencing and longevity protein Sir2 is an NAD-dependent histone deacetylase. *Nature.* 2000;403(6771):795–800.
23. Revollo JR, Grimm AA, Imai S. The NAD biosynthesis pathway mediated by nicotinamide phosphoribosyltransferase regulates Sir2 activity in mammalian cells. *J Biol Chem.* 2004;279(49):50754–50763.
24. Onyango P, Celic I, McCaffery JM, Boeke JD, Feinberg AP. SIRT3, a human SIR2 homologue, is an NAD-dependent deacetylase localized to mitochondria. *Proc Natl Acad Sci U S A.* 2002;99(21):13653–13658.
25. Scher MB, Vaquero A, Reinberg D. SirT3 is a nuclear NAD+-dependent histone deacetylase that translocates to the mitochondria upon cellular stress. *Genes Dev.* 2007;21(8):920–928.
26. Schwer B, North BJ, Frye RA, Ott M, Verdin E. The human silent information regulator (Sir)2 homologue hSIRT3 is a mitochondrial nicotinamide adenine dinucleotide-dependent deacetylase. *J Cell Biol.* 2002;158(4):647–657.
27. Shi T, Wang F, Stieren E, Tong Q. SIRT3, a mitochondrial sirtuin deacetylase, regulates mitochondrial function and thermogenesis in brown adipocytes. *J Biol Chem.* 2005;280(14):13560–13567.
28. Hallows WC, Lee S, Denu JM. Sirtuins deacetylate and activate mammalian acetyl-CoA synthetases. *Proc Natl Acad Sci U S A.* 2006;103(27):10230–10235.
29. Schwer B, Bunkenborg J, Verdin RO, Andersen JS, Verdin E. Reversible lysine acetylation controls the activity of the mitochondrial enzyme acetyl-CoA synthetase 2. *Proc Natl Acad Sci U S A.* 2006;103(27):10224–10229.
30. Ahn BH, et al. A role for the mitochondrial deacetylase Sirt3 in regulating energy homeostasis. *Proc Natl Acad Sci U S A.* 2008;105(38):14447–14452.
31. Lombard DB, et al. Mammalian Sir2 homolog SIRT3 regulates global mitochondrial lysine acetylation. *Mol Cell Biol.* 2007;27(24):8807–8814.
32. Tsai FC, Gardner DK. Nicotinamide, a component of complex culture media, inhibits mouse embryo development in vitro and reduces subsequent developmental potential after transfer. *Fertil Steril.* 1994;61(2):376–382.
33. Fato R, et al. Differential effects of mitochondrial Complex I inhibitors on production of reactive oxygen species. *Biochim Biophys Acta.* 2009; 1787(5):384–392.
34. Dumollard R, Duchen M, Carroll J. The role of mitochondrial function in the oocyte and embryo. *Curr Top Dev Biol.* 2007;77:21–49.
35. Kruse JP, Gu W. Modes of p53 regulation. *Cell.* 2009;137(4):609–622.
36. Vousden KH, Ryan KM. p53 and metabolism. *Nat Rev Cancer.* 2009;9(10):691–700.
37. Menendez D, Inga A, Resnick MA. The expanding universe of p53 targets. *Nat Rev Cancer.* 2009;9(10):724–737.
38. Riley T, Sontag E, Chen P, Levine A. Transcriptional control of human p53-regulated genes. *Nat Rev Mol Cell Biol.* 2008;9(5):402–412.
39. Han MK, Song EK, Guo Y, Ou X, Mantel C, Broxmeyer HE. SIRT1 regulates apoptosis and Nanog expression in mouse embryonic stem cells by controlling p53 subcellular localization. *Cell Stem Cell.* 2008;2(3):241–251.
40. Lin T, et al. p53 induces differentiation of mouse embryonic stem cells by suppressing Nanog expression. *Nat Cell Biol.* 2005;7(2):165–171.
41. Sundaresan NR, Samant SA, Pillai VB, Rajamohan SB, Gupta MP. SIRT3 is a stress-responsive deacetylase in cardiomyocytes that protects cells from stress-mediated cell death by deacetylation of Ku70. *Mol Cell Biol.* 2008;28(20):6384–6401.
42. Wallace DC, Fan W. The pathophysiology of mitochondrial disease as modeled in the mouse. *Genes Dev.* 2009;23(15):1714–1736.
43. Jacobs KM, et al. SIRT3 interacts with the daf-16 homolog FOXO3a in the mitochondria, as well as increases FOXO3a dependent gene expression. *Int J Biol Sci.* 2008;4(5):291–299.
44. Turrens JF. Mitochondrial formation of reactive oxygen species. *J Physiol.* 2003;552(pt 2):335–344.
45. Sundaresan NR, Gupta M, Kim G, Rajamohan SB, Isbatan A, Gupta MP. Sirt3 blocks the cardiac hypertrophic response by augmenting Foxo3a-dependent antioxidant defense mechanisms in mice. *J Clin Invest.* 2009;119(9):2758–2771.
46. Jin XL, Chandrakanthan V, Morgan HD, O'Neill C. Preimplantation embryo development in the mouse requires the latency of TRP53 expression,

which is induced by a ligand-activated PI3 kinase/AKT/MDM2-mediated signaling pathway. *Biol Reprod.* 2009;81(1):234–242.
47. Jones SN, Roe AE, Donehower LA, Bradley A. Rescue of embryonic lethality in Mdm2-deficient mice by absence of p53. *Nature.* 1995;378(6553):206–208.
48. Montes de Oca Luna R, Wagner DS, Lozano G. Rescue of early embryonic lethality in mdm2-deficient mice by deletion of p53. *Nature.* 1995; 378(6553):203–206.
49. Karawajew L, Rhein P, Czerwony G, Ludwig WD. Stress-induced activation of the p53 tumor suppressor in leukemia cells and normal lymphocytes requires mitochondrial activity and reactive oxygen species. *Blood.* 2005;105(12):4767–4775.
50. Favetta LA, Robert C, St John EJ, Betts DH, King WA. p66shc, but not p53, is involved in early arrest of in vitro-produced bovine embryos. *Mol Hum Reprod.* 2004;10(6):383–392.
51. Velez-Pardo C, Morales AT, Del Rio MJ, Olivera-Angel M. Endogenously generated hydrogen peroxide induces apoptosis via mitochondrial damage independent of NF-kappaB and p53 activation in bovine embryos. *Theriogenology.* 2007;67(7):1285–1296.
52. Jones RG, et al. AMP-activated protein kinase induces a p53-dependent metabolic checkpoint. *Mol Cell.* 2005;18(3):283–293.
53. Okoshi R, et al. Activation of AMP-activated protein kinase induces p53-dependent apoptotic cell death in response to energetic stress. *J Biol Chem.* 2008;283(7):3979–3987.
54. Luo J, et al. Negative control of p53 by Sir2alpha promotes cell survival under stress. *Cell.* 2001; 107(2):137–148.
55. Vaziri H, et al. hSIR2(SIRT1) functions as an NAD-dependent p53 deacetylase. *Cell.* 2001; 107(2):149–159.
56. Ito A, et al. p300/CBP-mediated p53 acetylation is commonly induced by p53-activating agents and inhibited by MDM2. *EMBO J.* 2001; 20(6):1331–1340.
57. Marchenko ND, Wolff S, Erster S, Becker K, Moll UM. Monoubiquitylation promotes mitochondrial p53 translocation. *EMBO J.* 2007;26(4):923–934.
58. Aida T, Oda S, Awaji T, Yoshida K, Miyazaki S. Expression of a green fluorescent protein variant in mouse oocytes by injection of RNA with an added long poly(A) tail. *Mol Hum Reprod.* 2001;7(11):1039–1046.

Development 137, 3823-3833 (2010) doi:10.1242/dev.054015

Endothelin receptor type A expression defines a distinct cardiac subdomain within the heart field and is later implicated in chamber myocardium formation

Rieko Asai[1], Yukiko Kurihara[1], Kou Fujisawa[1], Takahiro Sato[1], Yumiko Kawamura[1], Hiroki Kokubo[2,3], Kazuo Tonami[1], Koichi Nishiyama[1], Yasunobu Uchijima[1], Sachiko Miyagawa-Tomita[4] and Hiroki Kurihara[1,*]

SUMMARY

The avian and mammalian heart originates from two distinct embryonic regions: an early differentiating first heart field and a dorsomedially located second heart field. It remains largely unknown when and how these subdivisions of the heart field divide into regions with different fates. Here, we identify in the mouse a subpopulation of the first (crescent-forming) field marked by endothelin receptor type A (*Ednra*) gene expression, which contributes to chamber myocardium through a unique type of cell behavior. *Ednra-lacZ/EGFP*-expressing cells arise in the ventrocaudal inflow region of the early linear heart tube, converge to the midline, move anteriorly along the outer curvature and give rise to chamber myocardium mainly of the left ventricle and both atria. This movement was confirmed by fluorescent dye-labeling and transplantation experiments. The *Ednra-lacZ/EGFP*-expressing subpopulation is characterized by the presence of *Tbx5*-expressing cells. *Ednra*-null embryonic hearts often demonstrate hypoplasia of the ventricular wall, low mitotic activity and decreased *Tbx5* expression with reciprocal expansion of *Tbx2* expression. Conversely, endothelin 1 stimulates ERK phosphorylation and *Tbx5* expression in the early embryonic heart. These results indicate that early *Ednra* expression defines a subdomain of the first heart field contributing to chamber formation, in which endothelin 1/Ednra signaling is involved. The present finding provides an insight into how subpopulations within the crescent-forming (first) heart field contribute to the coordination of heart morphogenesis through spatiotemporally defined cell movements.

KEY WORDS: Cardiac development, Heart fields, Endothelin, Mouse

INTRODUCTION

The heart is the first functioning organ to develop during embryogenesis. Different sources of cell populations from the cardiogenic mesoderm and the cardiac neural crest coordinately contribute to the formation of elaborate cardiac structures, including the four specialized chambers, the valves and supporting tissues, and the conduction system (Buckingham et al., 2005; Cai et al., 2008; Kirby, 2007; Zhou et al., 2008). Myocardial progenitor cells first appear bilaterally in the anterior splanchnic mesoderm and move towards the midline to form the cardiac crescent and then the primary heart tube. Through subsequent growth by accretion of cells at the poles from a newly identified progenitor population called the second heart field (Cai et al., 2003; Galli et al., 2008; Kelly et al., 2001; Mjaatvedt et al., 2001; Waldo et al., 2001), the heart tube loops and in subsequent steps is sculpted into a four-chambered heart in mammals and birds (Abu-Issa and Kirby, 2007; Buckingham et al., 2005; Laugwitz et al., 2008).

[1]Department of Physiological Chemistry and Metabolism, Graduate School of Medicine, The University of Tokyo, 7-3-1 Hongo, Bunkyo-ku, Tokyo 113-0033, Japan. [2]Division of Mammalian Development, National Institute of Genetics, 1111 Yata, Mishima Shizuoka 411-8540, Japan. [3]Department of Genetics, The Graduate University for Advanced studies, 1111 Yata, Mishima Shizuoka 411-8540, Japan. [4]Division of Cardiovascular Development and Differentiation, Medical Research Institute, Department of Pediatric Cardiology, Tokyo Women's Medical University, 8-1 Kawada-cho, Shinjuku-ku, Tokyo 162-8666, Japan.

*Author for correspondence (kuri-tky@umin.ac.jp)

Accepted 3 September 2010

The distinction between these two heart fields is further supported by retrospective clonal analysis using recombinant *lacZ* labeling (Meilhac et al., 2004). This analysis, in embryonic day (E) 8.5 mouse embryos, revealed two distinct cell lineages with different patterns of regionalization in the heart tube. The first lineage contributed to all left ventricular myocardium, some of the right ventricular myocardium, the atrioventricular canal and both atria. The second lineage contributed to the outflow tract and all other myocardial regions except for the left ventricle. Notably, the second lineage appears to correspond roughly to the second heart field marked by *Islet1* (*Isl1* – Mouse Genome Informatics) expression in terms of regional contribution (Cai et al., 2003; Galli et al., 2008). The clonal analysis also revealed that the two cell lineages segregate from a common progenitor around the time of gastrulation (Meilhac et al., 2004). Based on these findings, the first lineage is postulated to segregate first from the common progenitor pool to form the heart tube (Buckingham et al., 2005).

Following their segregation, the heart fields are probably further regionalized and diversified into various cell types. However, it remains largely unknown when and how different subpopulations arise within these heart-forming fields and how they interact with each other to coordinate heart morphogenesis.

Endothelin 1 (Edn1)/endothelin receptor type A (Ednra) signaling is known to be involved in cardiovascular and craniofacial development (Clouthier et al., 1998; Kurihara et al., 1994; Ozeki et al., 2004; Sato et al., 2008a; Sato et al., 2008b). Mice deficient in Edn1/Ednra signaling exhibit aortic arch malformation and outflow anomalies, which are attributed to cardiac neural crest defects (Kurihara et al., 1995; Yanagisawa et al., 1998). Correspondingly, *Ednra* is expressed in cranial and

cardiac neural crest-derived mesenchymal cells (Clouthier et al., 1998; Kurihara et al., 1995; Maemura et al., 1996; Yanagisawa et al., 1998).

Recently, we established mice in which *lacZ* (which encodes β-galactosidase) and *EGFP* (which encodes enhanced green fluorescent protein) were introduced into the *Ednra* locus to recapitulate its endogenous expression (Sato et al., 2008a). Consequently, *lacZ/EGFP* expression emerged in the developing heart with a characteristic pattern. We then focused on this expression, expecting that it might lead to the identification of a novel myocardial subpopulation. Here, we demonstrate that early *Ednra-lacZ/EGFP* expression marks a subpopulation of the heart field with distinct regional identity. *Ednra-lacZ/EGFP*-positive cells are first localized in the ventral inflow region, move anteriorly along the outer curvature following the formation of the heart tube, and give rise to chamber myocardium. Dye-labeling and transplantation experiments confirmed this movement and contribution to chamber formation. We also observed developmental abnormalities in *Ednra*-null embryonic hearts, indicating the involvement of Edn1 as a mitotic factor in early cardiac development.

MATERIALS AND METHODS

Mice

$Ednra^{lacZ/+}$ (*lacZ* knock-in) mice have been described previously (Sato et al., 2008a). To generate mice carrying the $Ednra^{EGFP}$ (*EGFP* knock-in) allele, we performed Cre recombinase-mediated cassette exchange (RMCE) on $Ednra^{neo/+}$ embryonic stem (ES) cells in which an exchangeable floxed site was introduced into the *Ednra* locus as described previously (Sato et al., 2008a) (see Fig. S1 in the supplementary material). Briefly, the EGFP cassette excised from the pEGFP-N3 expression vector (Clontech) was introduced into the knock-in vector p66-2272 containing multiple cloning sites between *lox66* and *lox2272* (Araki et al., 2002). The resultant plasmids were transfected into $Ednra^{neo/+}$ ES cells with AxCANCre recombinant adenovirus expressing the recombinase Cre tagged with a nuclear localization signal under the control of the CAG promoter (Kanegae et al., 1995). Targeted ES clones were injected into ICR blastocysts to generate germline chimeras that were then crossed with ICR females. Mice were housed in an environmentally controlled room at 23±2°C, with a relative humidity of 50-60% and under a 12-hour light:12-hour dark cycle. Genotypes were determined by PCR on tail-tip or amnion DNA using primers specific for RMCE-mediated recombination. Embryonic ages were determined by timed mating with the day of the plug being E0.5. The number of somites was also used to estimate developmental stages from E7.8 to E8.5. All animal experiments were reviewed and approved by the University of Tokyo Animal Care and Use Committee.

β-Galactosidase staining

lacZ expression was detected by staining with X-Gal (5-bromo-4-chloro-3-indolyl β-D-galactoside) for β-galactosidase activity. Whole-mount and section staining were performed as described previously (Nagy et al., 2003).

Immunohistochemistry

Embryo cryosections (12 μm) were immunostained using the following antibodies: rat monoclonal anti-GFP (Nacalai Tesque, Kyoto, Japan; 1:200), rabbit anti-GFP (Medical and Biological Laboratories, Nagoya, Japan; 1:250), rabbit anti-Nkx2.5 (Santa Cruz, 1:250), mouse monoclonal anti-Isl1 (39.5D5; Developmental Studies Hybridoma Bank; 1:100), mouse monoclonal anti-myosin heavy chain (MHC) (MF20-c; Developmental Studies Hybridoma Bank; 1:100), rabbit anti-desmin (Progen Biotechnik, Heidelberg, Germany; 1:200), mouse monoclonal phycoerythrin (PE)-conjugated anti-CD31 (BD Pharmingen; 1:200), mouse monoclonal anti-BrdU (Calbiochem; 1:20) and rabbit anti-phosphohistone H3 (pHH3) (Ser10) (Upstate Biotechnology; 1:250). Signals were visualized with horseradish peroxidase- or FITC-conjugated secondary antibodies specific for the appropriate species. Some sections were treated with biotin-conjugated secondary antibodies and visualized using the VECTASTAIN ABC System (Vector Laboratories), streptavidin-FITC (Dako; 1:200) or streptavidin-TRITC (1:200, Beckman Coulter). Nuclei were visualized with TO-PRO-3 (Molecular Probes).

In situ hybridization

Whole-mount in situ hybridization was performed as described previously (Wilkinson, 1992). Sections (12 μm) were prepared from frozen embryos. Treatment for in situ hybridization was as described previously with minor modifications (Ishii et al., 1997). The *Ednra*, *Cited1*, *Tbx2* and *Bmp2* probes have been described previously (Kokubo et al., 2007; Sato et al., 2008a). Probes for *Nkx2.5* (*Nkx2-5* – Mouse Genome Informatics), *Mlc2a* (*Myl7* – Mouse Genome Informatics) and *Isl1* (GenBank accession numbers: NM_008700, NM_021459 and NM_022879, respectively) were prepared using RT-PCR. The *Tbx5* probe was obtained from V. E. Papaioannou (Chapman et al., 1996; Sato et al., 2008a). The *Cx40* (*Gja5* – Mouse Genome Informatics) probe was obtained from D. Gros (Delorme et al., 1997). The *ANF* (*Nppa* – Mouse Genome Informatics) probe was obtained from T. Watanabe (Koibuchi and Chin, 2007). The *Hand1* probe was from D. Srivastava (Srivastava et al., 1995).

Fluorescent dye labeling

Embryos from 6- or 7-somite stages were collected, transferred to DMEM/F12 containing 10% FCS, and injected with PKH67 (green) or PKH26 (red) fluorescent dyes (Sigma) using a needle drawn from glass capillary tubing in order to label cells in the *lacZ*- or *EGFP*-expressing or adjacent regions. Embryos were then placed in a 15-ml culture bottle containing 2 ml culture medium (50% rat serum plus 50% DMEM/F12) and rotated at 20 rpm at 37°C while being continuously supplied with a suitable concentration of O_2 (5 or 20%) and CO_2 (5%) balanced with N_2 for 30 hours. Labeled embryos were observed using a Leica MZFLIII stereomicroscope equipped with a Hamamatsu C4742-95 digital camera. Some embryos were fixed for X-gal staining. For whole-heart labeling, E8.25 (6- to 7-somite stage) embryos were incubated in DMEM/F12 with 1 μM SYTO16 (Molecular Probes), which stains the nuclei of live cells, at 37°C in 5% CO_2 for 30 minutes, and the heart tubes were excised.

Transplantation and explant culture experiment

Cardiac inflow tissues corresponding to the *Ednra-lacZ/EGFP*-positive region were excised from E8.25 (5- to 7-somite stage) embryos and transplanted into the same regions of recipient embryos (without removing their own inflow regions) using fine glass and tungsten needles. The *Ednra-EGFP*-positive tail regions were also transplanted as a control experiment. For transplantation of SYTO16-labeled cells, heart tubes were cut into three parts (outflow, ventricular and inflow regions) and were transplanted into the inflow regions of recipient embryos. Embryos were then placed in a collagen-coated 3.5-cm dish containing 500 μl α-MEM with 10% horse serum at 37°C in 5% CO_2 balanced with N_2 for 24 hours. Following culture, embryos were observed under a fluorescence microscope or fixed in 4% paraformaldehyde and subjected to immunostaining. For explant culture, dissected SYO16-labeled tissues were placed onto collagen-coated dishes and were incubated in α-MEM with 10% horse serum at 37°C in 5% CO_2 for 24 hours.

BrdU labeling

Pregnant female mice at E9.5 were injected intraperitoneally with bromodeoxyuridine (BrdU; 0.2 mg/g body weight; Sigma). After 1 hour of BrdU exposure, embryos were harvested on ice-cold PBS to stop BrdU incorporation and were fixed in 4% paraformaldehyde for 1 hour. Cryosections were treated with 2 M HCl and subjected to immunostaining with anti-BrdU antibody. For each sample, two sequential transverse sections through the widest region of the left and right ventricles were taken and BrdU-positive nuclei were counted in the compact, trabecular and endocardial layers of the ventricular wall. The sections were then counterstained with Hematoxylin to visualize nuclei and the total of

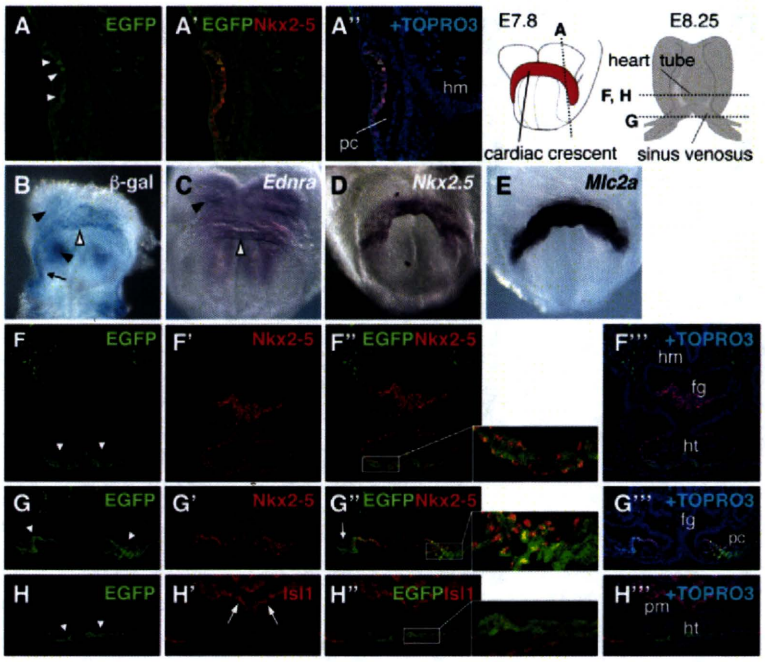

Fig. 1. *Ednra-lacZ/EGFP* expression in early developing hearts at the 1- to 4-somite stages. (**A-A″**) Sagittal sections of a 1-somite stage *Ednra-EGFP* mouse embryo immunostained for EGFP (A; green) and Nkx2.5 (A′; red), merged with TO-PRO-3 staining for nuclei (A″; blue). EGFP-positive cells were detected within the Nkx2.5-positive heart-forming region (white arrowheads). (**B**) Ventral view of a 3-somite stage *Ednra-lacZ* embryo stained for β-galactosidase activity. *lacZ*-expressing cells were detected within the cardiac crescent (white arrowhead), non-cardiogenic mesoderm (arrow) and head mesenchyme behind the crescent (black arrowheads). (**C-E**) Whole-mount in situ hybridization for *Ednra* (C), *Nkx2.5* (D) and *Mlc2a* (E) on a 3-somite stage embryo. White and black arrowheads indicate *Ednra* expression in the cardiac crescent and head mesenchyme, respectively. (**F-H‴**) Transverse sections of 4-somite stage *Ednra-EGFP* embryos immunostained for EGFP (F,G,H,F″,G″,H″) and Nkx2.5 (F′,F″,G′,G″) or Isl1 (H′,H″) with TO-PRO-3 staining (F‴,G‴,H‴). The boxed regions in F″,G″,H″ are magnified in the panels to the right. EGFP-positive cells were detected within the Nkx2.5-positive heart tube (arrowheads) and Nkx2.5-negative lateral plate mesoderm (arrow in G″). EGFP expression did not overlap with Isl1 expression in the second heart field (arrows in H′). Planes of sections are indicated in the diagrams at the top. fg, foregut; hm, head mesenchyme; ht, heart tube; pc, pericardial coelom; pm, pharyngeal mesoderm.

number nuclei was counted in order to calculate the ratio of BrdU-positive to total nuclei. Statistical significance ($P<0.05$) was determined using the paired *t*-test. Data are presented as mean±s.e.m.

Phosphorylation of ERK

Hearts were collected from E9.5 wild-type, *Ednra*$^{+/EGFP}$ and *Ednra*$^{EGFP/EGFP}$ embryos and lysed with lysis buffer [50 mM Tris-HCl (pH 8.0), 150 mM NaCl, 1 mM EDTA, 1% Triton X-100, 0.1% SDS, 0.1% sodium deoxycholate, protease inhibitor cocktail (Roche), 1 mM sodium orthovanadate and 1 mM sodium fluoride]. The lysates were subjected to SDS-PAGE and immunoblotted using a mouse monoclonal antibody to phosphorylated ERK1/2 and a rabbit polyclonal antibody to total ERK1/2 (both Cell Signaling Technology). To evaluate the effect of Edn1, E9.5 wild-type hearts were incubated in serum-free DMEM with or without 10 μM BQ123 (a cyclic peptide) for 3 hours then stimulated with 100 nM Edn1 for 5 minutes at 37°C. To evaluate the effect of BQ123 on basal ERK phosphorylation, E9.5 wild-type hearts were incubated in DMEM containing 10% fetal calf serum with or without 10 μM BQ123 for 3 hours. Signal intensity was quantified with ImageJ software (NIH). One-way analysis of variance (ANOVA) with Tukey's test was applied for comparisons of phosphorylated ERK levels among genotypes.

Conventional RT-PCR

Hearts were collected from E8.25 and E9.5 embryos and sorted into EGFP-positive and EGFP-negative cells using a FACS VantageSE (BD Biosciences). Total RNA was extracted from sorted fractions with the use of Isogen (Nippon Gene, Tokyo, Japan), and 1 μg samples were then reverse-transcribed using ReverTra Ace (Toyobo, Osaka, Japan) with oligo(dT) primer (Takara Bio, Shiga, Japan). The resulting cDNAs were amplified with Taq polymerase (Takara Bio) in a thermocycler. The sequences of the forward and reverse primers as well as the amplicon lengths are listed in Table S1 in the supplementary material. Custom primers were designed using Primer-BLAST online software (http://www.ncbi.nlm.nih.gov/tools/primer-blast/). Thermal cycling was performed for 25-30 cycles to maintain PCR conditions within the linear range of amplification before saturation was reached. Each cycle consisted of 30 seconds of denaturation at 94°C, 30 seconds of annealing at each annealing temperature (see Table S1 in the supplementary material) and 30 seconds of extension at 72°C. Glyceraldehyde-3-phosphate dehydrogenase (*Gapdh*) was used as an internal control.

Quantitative real-time RT-PCR

Left ventricles were isolated from E9.5 embryos. To evaluate the effect of Edn1, isolated ventricles were cultured in DMEM plus 5% fetal calf serum with or without 100 nM Edn1 for 24 hours. Total RNA was extracted from a pool of seven samples for each genotype or culture condition. Quantification of the amount of each mRNA was performed by real-time RT-PCR analyses using a LightCycler (Roche) and Real-Time PCR Premix with SYBR Green (RBC Bioscience) following the manufacturer's protocol. The primers and reaction conditions are shown in Table S1 in the supplementary material. Thermal cycling was performed for 47 cycles after incubation at 96°C for 10 minutes in at least three separate runs. Each cycle consisted of 10 seconds of denaturation at 95°C, 10 seconds of annealing at each annealing temperature (see Table S1 in the supplementary material) and 11 seconds of extension at 72°C. The second-derivative maximum method was adopted to determine the crossing points automatically for individual samples, and relative amounts of mRNA were calculated based on the crossing-point analysis. Hypoxanthine phosphoribosyltransferase (*Hprt*) was used as an internal control. The result was expressed as a fold change relative to the control. The Mann-Whitney *U*-test was applied for comparisons of relative mRNA levels between genotypes or culture conditions.

RESULTS

Ednra-lacZ/EGFP expression defines a distinct subdomain within the cardiac crescent

We characterized marker gene expression in the embryonic heart of *Ednra*$^{lacZ/+}$ and *Ednra*$^{EGFP/+}$ mice. *Ednra-lacZ/EGFP*-positive cells were first detected in the crescent-forming cardiogenic mesoderm around the 1-somite stage (~E7.8) (Fig. 1A-A″). At the 1- to 3/4-somite stages (E7.8~E8.0), *Ednra-lacZ* signals coincided with detection of endogenous expression of *Ednra* (Fig. 1B,C) and were colocalized with *Nkx2.5* and *Mlc2a* (Fig. 1A′,A″,D,E). Double immunostaining on sections revealed that *Ednra-EGFP* expression overlapped with *Nkx2.5* expression in the ventral region of the heart tube (Fig. 1F-F″). In the caudal region, *Ednra-lacZ/EGFP* expression extended to the *Nkx2.5*-negative lateral plate mesoderm (Fig. 1B,G-G″) and to the extra-embryonic mesoderm of the amnion along the border with the embryonic

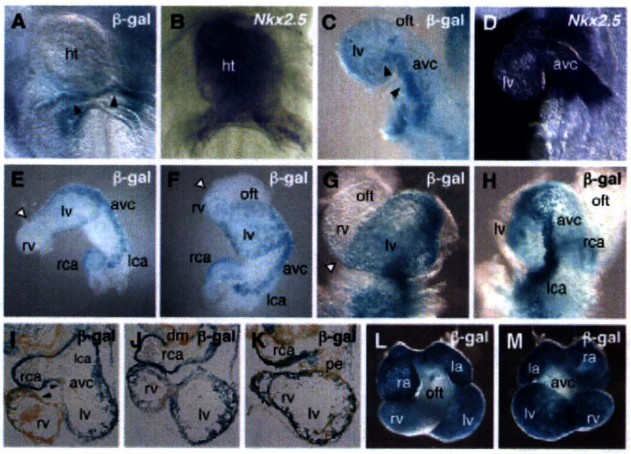

Fig. 2. β-Galactosidase staining and in situ hybridization for *Nkx2.5* on *Ednra-lacZ* hearts. (**A-D**) Hearts at 6/7- (A,B; ventral views) and 9/10- (C,D; left lateral views) somite stages, stained for β-galactosidase activity (A,C) or *Nkx2.5* expression (B,D). β-Galactosidase activity is most intense in the inflow region (arrowheads in A) and then extends towards the atrioventricular canal and left ventricle (arrowheads in C). (**E-H**) Dissected hearts at the 10- (E,F) and 13- (G,H) somite stages, stained for β-galactosidase activity and viewed from the inferior (E), ventral (F,G) and left-dorsal (H) sides. White arrowheads indicate boundaries of β-galactosidase expression. (**I-K**) Transverse sections of E9.5 *Ednra-lacZ* hearts stained for β-galactosidase activity. Sections are counterstained with Orange G. β-Galactosidase-positive cells contribute to all four chambers, but not to the atrioventricular canal and inner curvature. Arrowheads indicate expression boundaries along the inner curvature. Dorsal mesocardium and proepicardium were also negative for β-galactosidase activity. (**L,M**) Ventral (L) and dorsal (M) views of an E10.5 heart stained for β-galactosidase activity. avc, atrioventricular canal; dm, dorsal mesocardium; ht, heart tube; l/r(c)a, left/right (common) atrium; l/rv, left/right ventricle; oft, outflow tract; pe, proepicardium.

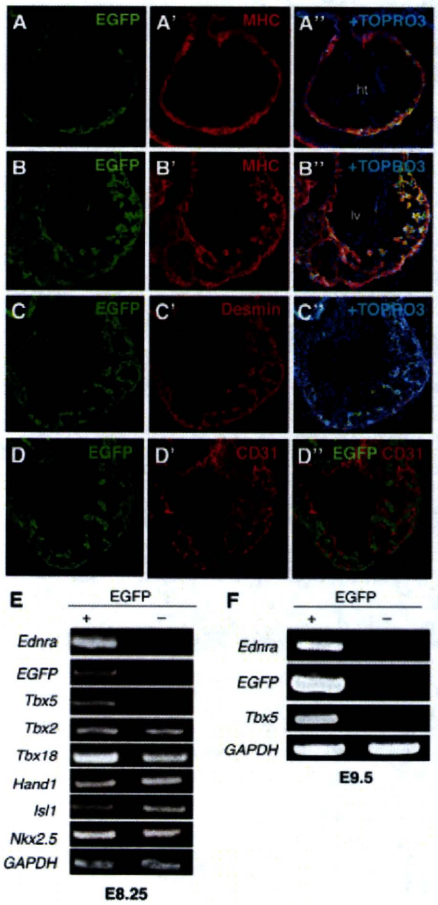

Fig. 3. Characterization of *Ednra-lacZ/EGFP*-expressing cells. (**A-D″**) Co-immunostaining for EGFP and cardiac markers in early *Ednra-EGFP* hearts. Transverse sections of E8.25 (7-somite stage; A-A″) and E9.5 (B-D″) *Ednra-EGFP* embryos immunostained for EGFP (A-D,D″) and myosin heavy chain (MHC; A′,B′), desmin (C′) or CD31 (D′,D″) with TO-PRO-3 staining (A″,B″,C″). ht, heart tube; lv, left ventricle. (**E,F**) RT-PCR analysis of *Ednra-EGFP*-positive and -negative cells from E8.25 (E) and E9.5 (F) hearts.

body. In contrast with its colocalization with *Nkx2.5*, *EGFP* expression never overlapped with *Isl1* expression, which marks the second heart field located behind the forming heart tube at this stage (Cai et al., 2003) (Fig. 1H-H″). These findings indicate that the *Ednra-lacZ/EGFP*-expressing cells might represent a myocardial subdomain within the first heart field.

Ednra-lacZ/EGFP-positive cells contribute to the chamber-forming myocardium

During linear tube formation at the 6/7-somite stage (~E8.25), *Ednra-lacZ* expression was largely confined to the caudal inflow region corresponding to the venous pole (Fig. 2A,B). Subsequently, *Ednra-lacZ* expression was extended to the left lateral wall of the looping heart, forming an apparent trajectory along the outer curvature (Fig. 2C,D). At the 10- to 13-somite stage (~E8.5), β-galactosidase-positive cells were distributed from the venous pole to the left ventricle through a narrow region within the left lateral wall of the atrioventricular canal and atria (Fig. 2E-H). By contrast, the dorsal side of the heart, along the inner curvature and the outflow tract, lacked β-galactosidase expression (Fig. 2E-H). In the right ventricle, only the caudal (posterior) region was populated by β-galactosidase-positive cells (Fig. 2F,G). These patterns were almost identical to the endogenous *Ednra* expression revealed by in situ hybridization (see Fig. S2 in the supplementary material). At E9.5, β-galactosidase-positive cells were distributed in the common atrium, left ventricle and a posterior part of the right ventricle (Fig. 2I-K). By contrast, the trabeculation-free region in the inner curvature, dorsal mesocardium and proepicardium lacked β-galactosidase expression (Fig. 2I-K). At E10.5, β-galactosidase was widely expressed in the four chambers, whereas the atrioventricular canal and outflow tract were mostly negative (Fig. 2L,M).

To confirm that *Ednra-lacZ/EGFP* expression marked the myocardial cell lineage, we examined myocardial marker expression. In the E8.25 heart tube and the E9.5 left ventricle, EGFP expression overlapped with myosin heavy chain expression (Fig. 3A,B). At E9.5, EGFP-expressing cells also expressed desmin (Fig. 3C), a marker for chamber-forming myocardium (Schaart et al., 1989). By contrast, EGFP expression did not overlap with CD31 expression, which marks endocardial cells (Fig. 3D). EGFP-expressing cells were further characterized by fluorescence-activated cell sorting (FACS) and RT-PCR. At E8.25 and E9.5, only EGFP-positive fractions expressed *Ednra* and *EGFP*. Remarkably, expression of *Tbx5*, a T-box transcription factor gene crucial for early heart development (Bruneau et al., 2001; Takeuchi et al.,

2003), was also only detected in EGFP-positive fractions (Fig. 3E,F). Section staining confirmed the presence of Tbx5-positive cells in the *Ednra-EGFP*-expressing region, particularly in the caudal inflow region (see Fig. S2 in the supplementary material). These results indicate that *Ednra-lacZ/EGFP* expression marks chamber-forming cardiomyocytes, including *Tbx5*-positive cells arising in the inflow region.

Dye injected into the ventral inflow region follows the subsequent distribution of the *Ednra-lacZ/EGFP*-positive subdomain

Extension of *Ednra-lacZ/EGFP* expression along the outer curvature raises the possibility that *Ednra-lacZ/EGFP*-expressing cells in the ventral inflow region move into the linear heart tube to give rise to chamber myocardium. However, it is also possible that *Ednra-lacZ/EGFP* expression is sequentially upregulated with different timing in cells already present in the heart tube. These possibilities are not mutually exclusive. To examine whether the upward cell movement contributes to the extension of *Ednra-lacZ/EGFP* expression, we injected PKH fluorescent dyes into the ventral inflow region and adjacent areas at the 6/7-somite stage and cultured the injected embryos for 30 hours. The injected areas, distribution patterns of labeled cells and summary of the results are shown in Fig. 4A. After 30 hours, labeled cells were found in the left lateral wall of the atrium and atrioventricular canal towards the left ventricle (I in Fig. 4A) in 13 out of 14 embryos in which dye was injected into the middle (a in Fig. 4A; n=6) or left (b in Fig. 4A; n=8) portion of the ventral inflow region (Fig. 4B-C′). Labeled cells were also found in the left ventricle in three embryos in which dye was injected into the middle region (Fig. 4B′). These results support the possibility of cell movement. Interestingly, five out of six embryos in which dye was injected into the right portion of the ventral inflow region (c in Fig. 4A) also had labeled cells in the contralateral left wall of the atrium and atrioventricular canal after 30 hours (Fig. 4D,D′). The one remaining embryo showed labeled cells in the future right atrium (Fig. 4E,E′). Thus, dye-injection experiments indicate that *lacZ/EGFP*-positive cells on both sides of the inflow region at the 6/7-somite stage contribute to the cell population extending to the left ventricle.

By contrast, only two out of 13 embryos in which dye was injected into the adjacent *lacZ/EGFP*-negative region revealed labeled cells in the atrial wall (Fig. 4A; d-g). In one of those embryos, labeled cells appeared in the left dorsocranial wall 30 hours after injection into the *lacZ/EGFP*-negative region dorsomedially adjacent to the left *lacZ/EGFP*-positive region (Fig. 4; f→III); in the other, labeled cells were detected in the right lateral wall after injection into the right *lacZ/EGFP*-negative region (Fig. 4; g→II). These distribution patterns are consistent with the previous report that cells in the right and left posterior second heart field contribute to the corresponding right and left wall of the atrium (Galli et al., 2008).

When transplanted, the *Ednra-lacZ/EGFP*-positive inflow region contributes to left ventricular and atrial myocardium

To confirm the movement from the ventral inflow region to the developing left ventricle and atrium, we transplanted, at E8.25 (5- to 7-somite stage), the *Ednra-lacZ/EGFP*-positive inflow region into the same region of wild-type embryos (Fig. 5A). After 24 hours, *Ednra-EGFP*-positive cells were detected in the left ventricle in five out of eight recipient embryos transplanted with the $Ednra^{EGFP/+}$ inflow region (Fig. 5B-B″). By contrast, no EGFP signals were

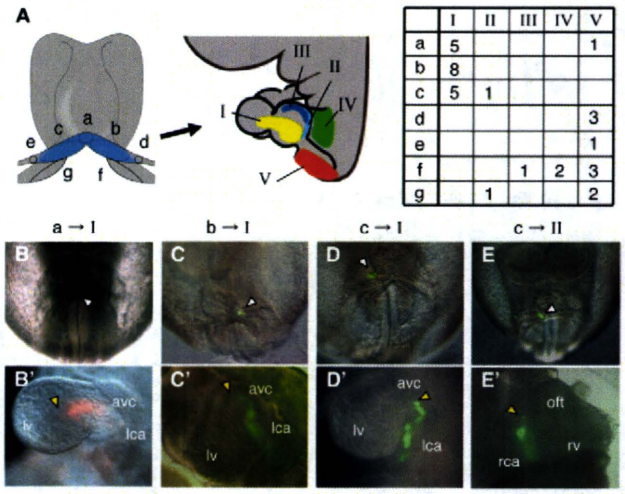

	I	II	III	IV	V
a	5				1
b	8				
c	5	1			
d					3
e					1
f			1	2	3
g		1			2

Fig. 4. PKH fluorescent dye injection into the inflow region. (**A**) Schematics indicating areas of injection (left) and distribution after 30 hours (middle). Table shows the number of embryos observed with dye present in each of the regions I-V following injection at each of the sites a-g. a/b/c, middle/left/right areas within the *Ednra-lacZ/EGFP*-positive region (blue); d/e, areas lateral to b/c; f/g, left/right areas dorsomedial to the *Ednra-lacZ/EGFP*-positive region; I, left lateral wall of the inflow tract; II, right common atrial wall; III, dorsocranial wall of the left common atrium; IV, region around the pharyngeal mesoderm; V, region around the lateral mesoderm. (**B-E′**) Representative results. Dye was injected at the sites indicated (white arrowheads in B-E) and traced after 30 hours (B′-E′). Yellow arrowheads indicate anterior boundaries of dye fluorescence. avc, atrioventricular canal; lca, left common atrium; lv, left ventricle; oft, outflow tract; rca, right common atrium.

detected when *Ednra-EGFP*-positive tails from $Ednra^{EGFP/+}$ embryos were transplanted (n=7; Fig. 5C-C″). No fluorescent signals were observed in the left ventricle of wild-type recipients transplanted with a wild-type inflow region (n=7; Fig. 5D-D″). $Ednra^{EGFP/+}$ recipients transplanted with the $Ednra^{EGFP/+}$ inflow region exhibited strong endogenous EGFP signals in the ventricle, as expected (n=6; Fig. 5E-E″).

To verify further the regional specificity with respect to movement, we transplanted different regions of the E8.25 heart tube, labeled with SYTO16 fluorescent dye, into the inflow region of the heart at the same developmental stage (Fig. 5F). When SYTO16-labeled cells were transplanted into the outflow or ventricular region, no upward movement was detected after 24 hours (n=5 for each; Fig. 5G-G″,H-H″). By contrast, SYTO16-labeled cells were found to distribute along the outer curvature towards the left ventricle after 24 hours in all five embryos transplanted with cells in the inflow region (Fig. 5I-I″). These results strongly support the movement and contribution of *Ednra-lacZ/EGFP*-positive inflow cells to the developing left ventricle.

As indicated by β-galactosidase staining, *Ednra-lacZ/EGFP* was widely expressed in the four chambers after E9.5, raising the possibility that many *Ednra*-negative cells in the early heart tube might become *Ednra*-positive at later stages. To test this idea, we performed explant culture of the ventricular and inflow regions of the E8.25 heart tube separately. At the start of culture, EGFP signals were clearly detectable in the inflow region, but were very low in the ventricle (see Fig. S3 in the supplementary material). After 24 hours, ventricular and inflow regions both demonstrated

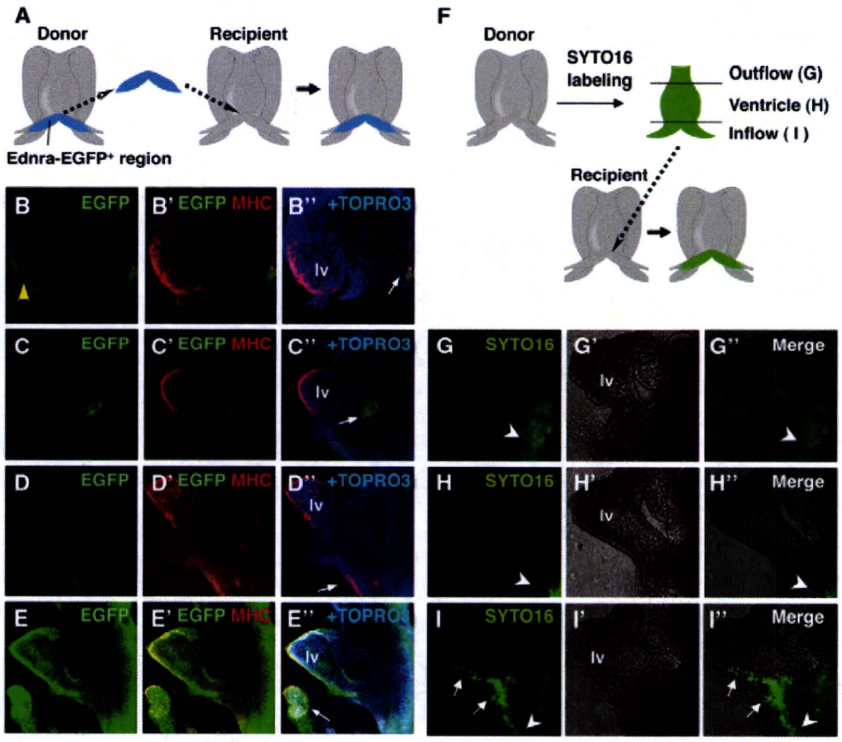

Fig. 5. Transplantation of the ventral inflow region. (**A**) Schematic indicating transplantation of the *Ednra-EGFP*-positive ventral inflow region. (**B-E″**) Representative results 24 hours after transplantation of the inflow region (B-B″,D-E″) or the tail region (C-C″) from $Ednra^{EGFP/+}$ (B-C″,E-E″) or wild-type (D-D″) embryos into the same region of wild-type (B-D″) or $Ednra^{EGFP/+}$ (E-E″) embryos. White arrows, transplants; yellow arrowhead, EGFP signals in the left ventricle (lv). (**F**) Schematic indicating transplantation of SYTO16-labeled heart regions. (**G-I″**) Representative results 24 hours after transplantation of the outflow (G-G″), ventricular (H-H″) and inflow (I-I″) regions. SYTO16 signals (G,H,I) and optical images (G′,H′,I′) are superimposed in G″, H″ and I″. Arrowheads, areas of transplantation; arrows, SYTO16-labeled cells along the outer curvature towards the left ventricle (lv).

intense EGFP signals (see Fig. S3 in the supplementary material). These results suggest that tube-forming cells that are *Ednra* negative at early stages might start to express *Ednra* later.

Defects in ventricular chamber formation in *Ednra*-null mice

In addition to outflow abnormalities as a result of cardiac neural crest defects, some *Edn1*-null embryos from Edn antagonist-treated pregnant mice exhibited ventricular hypoplasia (Kurihara et al., 1995), indicating involvement of Edn signaling in cardiac chamber development. To investigate this further, we revisited the *Ednra*-null phenotype.

At E9.5, when cardiac neural crest cells are not yet seen in the conus arteriosus (Jiang et al., 2000), $Ednra^{lacZ/EGFP}$ (*Ednra*-null) embryos were obtained at the expected Mendelian ratio (49:102:56 wild-type:heterozygous:null). Of the 43 $Ednra^{lacZ/EGFP}$ embryos examined, 26 (60%) showed normally developed hearts (Fig. 6A,B). By contrast, 17 $Ednra^{lacZ/EGFP}$ embryos (40%) showed a gourd-shaped heart with disproportionate chamber sizes (Fig. 6C). These morphological changes indicate that Ednra-mediated signals might be involved in normal growth during chamber formation. To further characterize the *Ednra*-null phenotype, we compared the distribution of β-galactosidase-positive cells in the hearts of $Ednra^{lacZ/+}$ and $Ednra^{lacZ/EGFP}$ embryos at E9.5. β-galactosidase expression in the caudal (posterior) ventricular wall tended to distribute from left to right to a lesser extent in $Ednra^{lacZ/EGFP}$ embryos than in $Ednra^{lacZ/+}$ littermates (see Fig. S4 in the supplementary material). Histological examination revealed that $Ednra^{lacZ/EGFP}$ embryos often had a poorly developed ventricular wall with a low distribution of β-galactosidase-positive cells (Fig. 6D-G).

Next, we performed BrdU labeling to examine whether the *Ednra*-null phenotype was associated with changes in proliferation. The number of proliferative cells incorporating BrdU was significantly decreased in the compact and trabecular layers of the ventricular wall of *Ednra*-null embryos compared with those of heterozygous $Ednra^{+/EGFP}$ embryos (Fig. 6H-M). Decreased BrdU uptake in the right ventricle could possibly be explained by low proliferation rates of β-galactosidase-positive cells populated in the caudal (posterior) region (Fig. 2F,G). Indeed, in the right ventricular region, the number of BrdU-labeled cells with a low β-galactosidase-positive population was similar in *Ednra*-null and heterozygous embryos (data not shown). To confirm this, we double stained serial ventricular sections for β-galactosidase activity and phosphohistone H3 (pHH3), a marker of mitosis (Cimini et al., 2003), and counted pHH3-positive cells separately in populations positive and negative for β-galactosidase. The mitotic frequency of β-galactosidase-positive, but not β-galactosidase-negative, cells was decreased in the left and right ventricles of the *Ednra*-null heart (Fig. 6N). Decreased BrdU incorporation in the endocardium of the $Ednra^{lacZ/EGFP}$ right ventricle is likely to be an indirect effect because the endocardial layer does not express *Ednra-lacZ*. We did not observe differences in the proportion of apoptotic cells between *Ednra*-null and heterozygous or wild-type embryos (data not shown).

Edn1 has been reported to act as a mitogen on cardiomyocytes by stimulating ERK phosphorylation (Sugden, 2003). We therefore examined ERK phosphorylation in E9.5 wild-type, $Ednra^{+/EGFP}$ and $Ednra^{lacZ/EGFP}$ hearts. ERK phosphorylation levels were decreased in proportion to the number of *Ednra*-null alleles (Fig. 7A,B). In E9.5 hearts in vitro, stimulation of ERK phosphorylation by Edn1 was abolished by the Ednra antagonist BQ123 (Fig. 7C). Basal ERK phosphorylation was also decreased by BQ123 (Fig. 7D). Taken together, these results suggest that the Ednra signal is involved in myocardial development as a mitogenic factor at early stages. By contrast, no differences in ERK phosphorylation were observed at E10.5 (data not shown), indicating that the negative effect of the *Ednra*-null mutation on myocardial proliferation might be overcome by other factors at later stages.

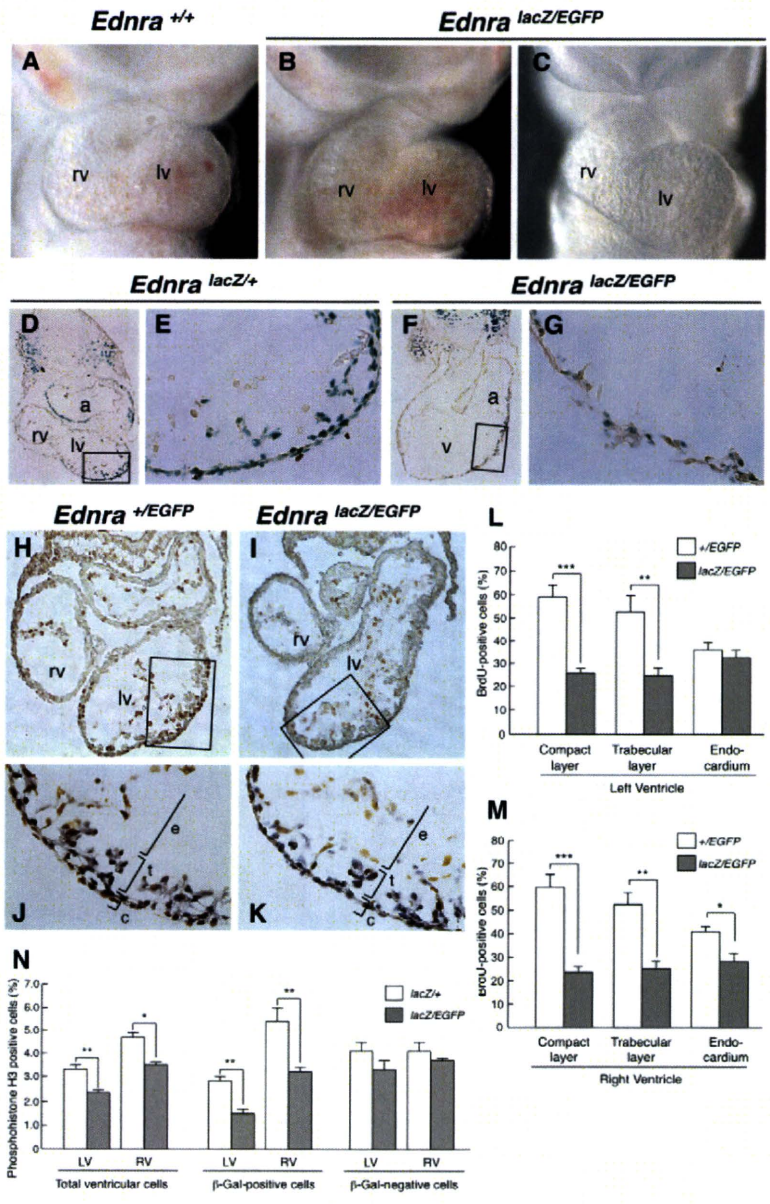

Fig. 6. Morphological, histological and cell proliferation analysis of *Ednra*-null hearts. (**A-C**) Representative wild-type (A) and *Ednra*$^{lacZ/EGFP}$ (*Ednra*-null) (B,C) hearts at E9.5. *Ednra*$^{lacZ/EGFP}$ embryo hearts appear normal (B) or gourd-shaped with disproportionate chamber sizes (C). (**D-G**) Representative transverse sections of E9.25 *Ednra*$^{lacZ/+}$ (D,E) and *Ednra*$^{lacZ/EGFP}$ (F,G) hearts stained for β-galactosidase activity. The boxed areas in D and F are magnified in E and G, respectively. The *Ednra*$^{lacZ/EGFP}$ heart is defective in ventricular wall formation and distribution of β-galactosidase-positive cells. (**H-K**) Representative transverse sections of BrdU-labeled (brown) *Ednra*$^{+/EGFP}$ (H,J) and *Ednra*$^{lacZ/EGFP}$ (I,K) hearts at E9.5. The boxed areas in H and I are magnified in J and K, respectively, after co-staining with Hematoxylin to visualize nuclei (purple). (**L,M**) Quantification of cell proliferation indicated by the ratio of BrdU-positive cells to total cell number in different compartments of the left (L) and right (M) ventricular wall of E9.5 *Ednra*$^{+/EGFP}$ and *Ednra*$^{lacZ/EGFP}$ hearts (n=3 for each). (**N**) Quantification of the percentage of phosphohistone H3-positive cells in the left (LV) and right (RV) ventricles of E9.5 *Ednra*$^{lacZ/+}$ and *Ednra*$^{lacZ/EGFP}$ hearts (n=3 for each) with respect to the numbers of β-galactosidase-positive, β-galactosidase-negative and total cells in three serial sections. Data are presented as mean±s.e.m. *P<0.05, **P<0.01, ***P<0.001. a, atrium; c, compact layer; e, endocardium; lv, left ventricle; rv, right ventricle; t, trabecular layer; v, ventricle.

Changes in T-box transcription factor gene expression in *Ednra*-null hearts

To examine whether the *Ednra*-null mutation affected gene expression in the early developing heart, we performed in situ hybridization for several marker genes on E9.5 *Ednra*$^{+/EGFP}$ and *Ednra*$^{lacZ/EGFP}$ hearts. *Ednra*$^{lacZ/EGFP}$ left ventricles showed decreased expression of *Tbx5* and its downstream gene *Cx40* (Fig. 8A,B), whereas the expression of other chamber myocardium markers such as *ANF*, *Hand1*, *Cited1* and *Mlc2a* was not affected (Fig. 8C-F). Decreased mRNA levels of *Tbx5* and *Cx40*, but not *Hand1*, were also confirmed by quantitative RT-PCR (Fig. 8G). Furthermore, *Tbx5* mRNA levels were increased by Edn1 in excised E9.5 heart explants (Fig. 8H).

The effect of the *Ednra*-null mutation on gene expression patterns was examined further by whole-mount in situ hybridization. In E8.25 *Ednra*$^{+/EGFP}$ and *Ednra*$^{lacZ/EGFP}$ hearts, *Tbx5* expression in the inflow region had a similar pattern to that of *Ednra* (Fig. 9A). At E9.5, *Tbx5* expression was expanded anteriorly towards the left ventricle in *Ednra*$^{+/EGFP}$ embryos (Fig. 9B), as described previously (Bruneau et al., 1999). This anterior expansion of *Tbx5* expression was decreased in *Ednra*$^{lacZ/EGFP}$ hearts, whereas *Tbx5* expression in the posterior (inflow) region was similar to that of *Ednra*$^{+/EGFP}$ embryos (Fig. 9C). By contrast, the *Tbx2*-expressing region, which normally corresponds to the atrioventricular canal (Aanhaanen et al., 2009), was reciprocally expanded in *Ednra*$^{lacZ/EGFP}$ hearts (Fig. 9D,E). *Bmp2* expression in the atrioventricular canal was similar in *Ednra*$^{+/EGFP}$ and *Ednra*$^{lacZ/EGFP}$ hearts (Fig. 9F,G), indicating that the expansion of *Tbx2* expression was independent of Bmp2, an inducer of *Tbx2* in the atrioventricular canal (Kokubo et al., 2007; Yamada et al., 2000). These results indicate that Edn1/Ednra signaling might be involved in the regulation of T-box transcription factor gene expression in early developing hearts.

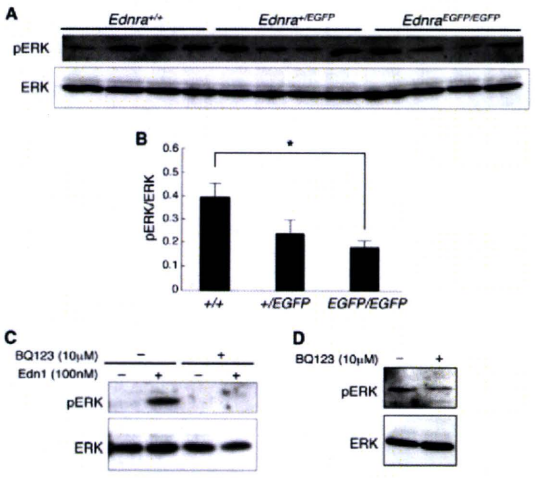

Fig. 7. Analysis of ERK phosphorylation. (**A**) Western blot of individual hearts excised from E9.5 wild-type, *Ednra*$^{+/EGFP}$ and *Ednra*$^{EGFP/EGFP}$ embryos using antibodies to phosphorylated (pERK) and total ERK1/2 (ERK). (**B**) Quantification of the ratio of phosphorylated to total ERK protein levels in A, normalized to control (wild-type) samples (n=5 per group). Data are presented as mean±s.e.m. *P<0.05. (**C**) Edn1 stimulates ERK phosphorylation in isolated E9.5 hearts. Edn1-induced ERK phosphorylation is completely abolished by the Ednra antagonist BQ123. (**D**) BQ123 downregulates basal ERK phosphorylation in isolated E9.5 hearts.

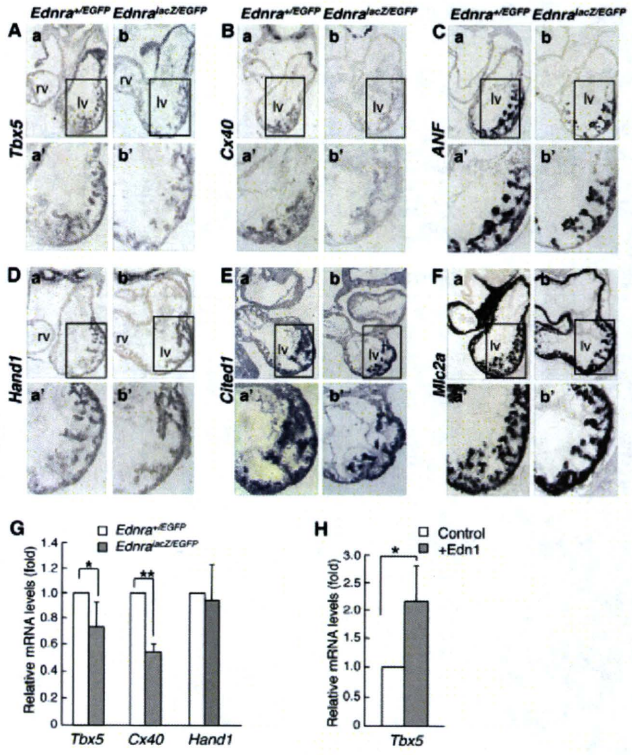

Fig. 8. Gene expression analysis of E9.5 *Ednra*-null hearts. (**A-F**) In situ hybridization of *Ednra*$^{+/EGFP}$ (a,a′) and *Ednra*$^{lacZ/EGFP}$ (b,b′) hearts for *Tbx5* (A), *Cx40* (B), *ANF* (C), *Hand1* (D), *Cited1* (E) and *Mlc2a* (F). a′ and b′ are magnifications of the regions indicated in a and b, respectively. lv, left ventricle; rv, right ventricle. (**G**,**H**) Real-time RT-PCR analysis. (G) *Tbx5* and *Cx40*, but not *Hand1*, expression levels are lower in *Ednra*$^{lacZ/EGFP}$ hearts than in *Ednra*$^{+/EGFP}$ hearts (n=5 per group). (H) In E9.5 wild-type ventricles, *Tbx5* expression is upregulated by stimulation with 100 nM Edn1 for 24 hours (n=4 per group). Data are presented as mean±s.e.m. *P<0.05, **P<0.01.

DISCUSSION

Regionalization of the first heart field and contribution to chamber formation

Here, we identified an *Ednra-lacZ/EGFP*-expressing cell population that is first detected in the cardiac crescent. At the early heart tube-forming stage, these cells are present in the ventral inflow region. Subsequently, dye-labeling experiments indicate that they move upward along the outer curvature between the 6/7-somite and 9/10-somite stages. This timing corresponds to the start of looping just after the formation of the linear heart tube (Abu-Issa and Kirby, 2007), indicating that the linear heart tube is mainly composed of *Ednra*-negative cells and that the *Ednra*-positive cells are recruited into the looping heart tube. This upward cell movement was confirmed and was shown to be specific for cells in the inflow region by dye-labeling and transplantation experiments. These findings suggest that *Ednra*-positive cells arising from the crescent-forming first heart field are a distinct subpopulation and contribute to chamber formation in a manner different from that of the early tube-forming cells.

de la Cruz and colleagues have performed extensive in vivo labeling experiments in the chick and showed that the inflow region between the interventricular grooves and the caudal end of the linear heart tube contributes to the trabeculated portion of the left ventricle (de la Cruz et al., 1989). The present study identified cells in the ventral wall within this inflow region as a subpopulation with a distinct gene expression signature and cell movement; cells at both sides converge to the midline and move upward along the outer curvature. In the chick embryo, the outer curvature is formed by the ventral seam after fusion of the bilateral cardiogenic fields (Abu-Issa and Kirby, 2008). Although in the chick embryo, unlike in the mouse, the bilateral heart fields remain separate until the tube-forming stage without forming the cardiac crescent, the mode of outer curvature formation by midline convergence of bilateral cells might be common to chick and mouse embryos.

The *Ednra-lacZ/EGFP*-expressing cell population is characterized by the presence of cells that express *Tbx5*, which is expressed in a posterior-to-anterior gradient in the inflow region and is important for left ventricular identity (Hoogaars et al., 2007). The *Ednra*-expressing region is distinct from the second heart field, marked by *Isl1* expression. However, *Isl1* expression was detected in both *Ednra-EGFP*-positive and -negative cells at E8.25 in our FACS and RT-PCR experiment. Recently, van den Berg et al. reported that, in chick, an *Isl1*-positive proliferating center caudodorsal to the inflow tract provides cells to the venous and arterial poles of the elongating heart tube (van den Berg et al., 2009). Apparently, *Ednra-lacZ/EGFP*-positive cells are distinct from this population because they are localized to the ventral region of the inflow and are *Isl1*-negative at the crescent/tube-forming stages. However, *Ednra-lacZ/EGFP*-positive cells might also be derived from the *Isl1*-positive pool as *Isl1* is initially expressed in all cardiogenic mesoderm and is downregulated on differentiation (Prall et al., 2007; Yuan and Schoenwolf, 2000). At later stages, many atrial cells express *Ednra-lacZ/EGFP*, suggesting that the second heart field-derived cells may also start to express this gene

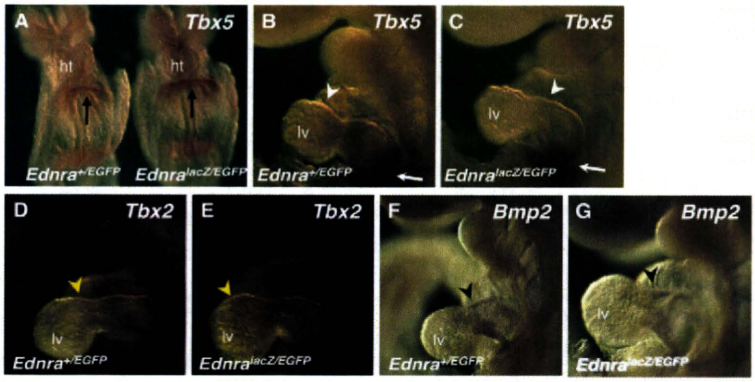

Fig. 9. Changes in *Tbx5* and *Tbx2* expression patterns in *Ednra*-null hearts. (**A**) In situ hybridization of E8.25 $Ednra^{+/EGFP}$ and $Ednra^{lacZ/EGFP}$ hearts. *Tbx5* expression in the inflow region was similar in both hearts (arrows). (**B-G**) In situ hybridization of E9.5 $Ednra^{+/EGFP}$ (B,D,F) and $Ednra^{lacZ/EGFP}$ (C,E,G) hearts for *Tbx5* (B,C), *Tbx2* (D,E) and *Bmp2* (F,G). Anterior expansion of *Tbx5* expression (white arrowheads) was decreased in $Ednra^{lacZ/EGFP}$ hearts, whereas *Tbx5* expression in the posterior (inflow) region (arrows) was similar. By contrast, the *Tbx2*-expressing region (yellow arrowheads) was expanded in $Ednra^{lacZ/EGFP}$ hearts. *Bmp2* expression in the atrioventricular canal (black arrowheads) was similar in $Ednra^{+/EGFP}$ and $Ednra^{lacZ/EGFP}$ hearts. ht, heart tube; lv, left ventricle.

at a later time than do first heart field-derived cells. Thus, *Isl1*-positive cells may eventually express *Ednra*, but the timing might be different between cardiac regions. Indeed, explant culture experiments revealed that *Ednra*-negative cells in the early heart tube might become *Ednra*-positive at later stages, indicating that later *Ednra*-positive cardiomyocytes are derived both from early *Ednra*-positive inflow cells and from tube-forming cells that are *Ednra*-negative at early stages.

According to the ballooning model for chamber formation, which is now widely accepted, the ventricular chambers bulge from the outer curvature of the looped heart (Christoffels et al., 2000). The developing chambers show high proliferative activity and are characterized by the upregulation of chamber-specific myocardial genes. A two-step model has been proposed for this process: the first step is the formation of a primary heart tube and the second step involves localized chamber differentiation in the ventral side (outer curvature) of the heart tube while primary myocardium is continuously recruited at arterial and venous poles of the tube (Christoffels et al., 2000; Moorman and Christoffels, 2003). However, it was not clear when and how chamber-forming cells in the outer curvature are specified. The present study suggests that *Ednra*-positive inflow cells might constitute part of the outer curvature by upward movement and contribute to chamber formation.

Dye-labeling experiments indicated that *Ednra*-positive cells along the outer curvature are derived from the bilateral inflow region. This implies that cells of both sides meet in the midline and distribute mainly to the left lateral wall as a mixed population. Dye labeling also demonstrated a contribution of *Ednra*-positive cells to the right atrial myocardium, although less frequently than to the left atrium. Galli et al. have demonstrated that the left and right sides of the posterior regions of the second heart field contribute to the left and right atrium, respectively (Galli et al., 2008). Thus, the atrial myocardium seems to be derived from at least two different cell sources in a different manner.

Role of endothelin signaling in early heart development

The present study characterizes further the *Ednra*-null phenotype in the early embryonic heart. Ventricular hypoplasia and associated decreased proliferation rates in *Ednra*-null hearts at E9.5 indicate that Ednra-mediated signals are involved in myocardial growth and ventricular formation. Around this stage, Edn1 is secreted by the endothelia of the outflow tract and adjacent vessels (Kurihara et al., 1995) and might act on Ednra-expressing cells arising from the inflow tract in a paracrine manner.

The present result appears to be contradictory to a previous report in which a cardiomyocyte-specific *Ednra*-knockout resulted in no detectable phenotype (Kedzierski et al., 2003). This discrepancy might be explained by the time lag between the start of *Ednra* expression (~E7.8) and myosin heavy chain promoter-driven Cre activation (E8.5-E9.5) (Eckardt et al., 2006; Niu et al., 2005), which might permit *Ednra* expression at early stages. Although it is still possible that the phenotype we describe is an indirect effect of the *Ednra*-null phenotype in other tissues, decreased mitotic frequency in β-galactosidase-positive cells, but not in β-galactosidase-negative cells, of the *Ednra*-null heart supports the possibility that the phenotype is the result of a direct effect on early cardiomyocytes through the Ednra signaling pathway.

The Edn1/Ednra signal is known to induce hypertrophic growth of cardiac myocytes through G_q/G_{11}-mediated activation of the ERK pathway (Sugden, 2003). Consistently, ERK phosphorylation tended to decrease in E9.5 *Ednra*-null hearts and was stimulated by Edn1 treatment. G_q/G_{11}-deficient embryos have severe myocardial hypoplasia in both the compact and trabecular layers, which might account for the mid-gestation lethality of these embryos (Offermanns et al., 1998). These findings lead us to speculate that Edn1/Ednra might be involved in the activation of a G_q/G_{11}-mediated mitotic pathway crucial for early myocardial development.

In addition, *Tbx5* and *Cx40* expression was downregulated in *Ednra*-null hearts and upregulated by stimulation with Edn1. Recent studies have implicated Tbx5 in the regulation of myocardial growth and proliferation (Georges et al., 2008; Goetz et al., 2006) and expression of *Tbx5* is affected by growth factors (Georges et al., 2008). Given these findings, it would be interesting to investigate further the relationship between Edn1/Ednra signaling and Tbx5-dependent myocardial growth/proliferation and chamber specification. Conversely, *Tbx2* expression was expanded towards the left ventricle without changes in *Bmp2* expression in *Ednra*-null hearts. Recently, Aanhaanen et al. reported that *Tbx2*-expressing cells arising in the bilateral limbs of the crescent contribute to the atrioventricular canal and, subsequently, to the *Tbx2*-negative left ventricle, particularly to the basal free wall where *Tbx2* expression is lost (Aanhaanen et al., 2009). In *Tbx2*-null hearts, the atrioventricular canal differentiates prematurely to chamber myocardium and proliferates at increased rates similar to that of chamber myocardium, indicating that Tbx2 might regulate the timing of chamber myocardial differentiation of *Tbx2*-expressing cells allocated to the left ventricular free wall (Aanhaanen et al., 2009). Considering that the *Ednra-lacZ/EGFP*-

positive cell population of the E8.25 heart expresses both *Tbx5* and *Tbx2*, these results raise the possibility that Edn1/Ednra signaling might be involved in chamber formation through the regulation of T-box transcription factor gene expression.

Relationship between cell populations expressing *Ednra* at early and late stages in cardiac development

The present study has revealed that *Ednra-lacZ/EGFP*-expressing cells represent a distinct subset of the first heart field and of the inflow region of the heart, contributing to chamber myocardial formation. Identification of this population has revealed novel aspects of early cell behavior contributing to heart morphogenesis. It has also shown an expansion of *Ednra* expression within chamber-forming cardiomyocytes and implicates the Ednra signal as a mitotic factor and potential regulator of T-box transcription factor gene expression in early cardiac development. The present experiments, investigating cellular distribution/movement and gene expression profiles, indicate that the early *Ednra*-expressing cells contribute partly to the late *Ednra*-expressing population together with cardiomyocytes, which start to express *Ednra* around E9.5 or later. These findings might provide new insight into the understanding of normal cardiac development, which is relevant to the pathogenesis of congenital heart diseases involving abnormalities of chamber morphogenesis.

Acknowledgements

We thank Margaret Buckingham and Margaret Kirby for helpful discussions and comments. We also thank Yuko Fujisawa and Sakura Kushiyama for technical assistance. R.A. is a Research Fellow of the Japan Society for the Promotion of Science (DC1). This work was supported in part by: Global COE Program (Integrative Life Science Based on the Study of Biosignaling Mechanisms), MEXT, Japan; grants-in-aid for scientific research from the Ministry of Education, Culture, Sports, Science and Technology, Japan; grants-in-aid for scientific research from the Ministry of Health, Labour and Welfare of Japan; Mitsubishi Pharma Research Foundation; Japan Cardiovascular Research Foundation; and Mochida Memorial Foundation for Medical and Pharmaceutical Research.

Competing interests statement

The authors declare no competing financial interests.

Supplementary material

Supplementary material for this article is available at http://dev.biologists.org/lookup/suppl/doi:10.1242/dev.054015/-/DC1

References

Aanhaanen, W. T., Brons, J. F., Dominguez, J. N., Rana, M. S., Norden, J., Airik, R., Wakker, V., de Gier-de Vries, C., Brown, N. A., Kispert, A. et al. (2009). The Tbx2+ primary myocardium of the atrioventricular canal forms the atrioventricular node and the base of the left ventricle. *Circ. Res.* **104**, 1267-1274.

Abu-Issa, R. and Kirby, M. L. (2007). Heart field: from mesoderm to heart tube. *Annu. Rev. Cell Dev. Biol.* **23**, 45-68.

Abu-Issa, R. and Kirby, M. L. (2008). Patterning of the heart field in the chick. *Dev. Biol.* **319**, 223-233.

Araki, K., Araki, M. and Yamamura, K. (2002). Site-directed integration of the cre gene mediated by Cre recombinase using a combination of mutant lox sites. *Nucleic Acids Res.* **30**, e103.

Bruneau, B. G., Logan, M., Davis, N., Levi, T., Tabin, C. J., Seidman, J. G. and Seidman, C. E. (1999). Chamber-specific cardiac expression of Tbx5 and heart defects in Holt-Oram syndrome. *Dev. Biol.* **211**, 100-108.

Bruneau, B. G., Nemer, G., Schmitt, J. P., Charron, F., Robitaille, L., Caron, S., Conner, D. A., Gessler, M., Nemer, M., Seidman, C. E. et al. (2001). A murine model of Holt-Oram syndrome defines roles of the T-box transcription factor Tbx5 in cardiogenesis and disease. *Cell* **106**, 709-721.

Buckingham, M., Meilhac, S. and Zaffran, S. (2005). Building the mammalian heart from two sources of myocardial cells. *Nat. Rev. Genet.* **6**, 826-835.

Cai, C. L., Liang, X., Shi, Y., Chu, P. H., Pfaff, S. L., Chen, J. and Evans, S. (2003). Isl1 identifies a cardiac progenitor population that proliferates prior to differentiation and contributes a majority of cells to the heart. *Dev. Cell* **5**, 877-889.

Cai, C. L., Martin, J. C., Sun, Y., Cui, L., Wang, L., Ouyang, K., Yang, L., Bu, L., Liang, X., Zhang, X. et al. (2008). A myocardial lineage derives from Tbx18 epicardial cells. *Nature* **454**, 104-108.

Chapman, D. L., Garvey, N., Hancock, S., Alexiou, M., Agulnik, S. I., Gibson-Brown, J. J., Cebra-Thomas, J., Bollag, R. J., Silver, L. M. and Papaioannou, V. E. (1996). Expression of the T-box family genes, Tbx1-Tbx5, during early mouse development. *Dev. Dyn.* **206**, 379-390.

Christoffels, V. M., Habets, P. E., Franco, D., Campione, M., de Jong, F., Lamers, W. H., Bao, Z. Z., Palmer, S., Biben, C., Harvey, R. P. et al. (2000). Chamber formation and morphogenesis in the developing mammalian heart. *Dev. Biol.* **223**, 266-278.

Cimini, D., Mattiuzzo, M., Torosantucci, L. and Degrassi, F. (2003). Histone hyperacetylation in mitosis prevents sister chromatid separation and produces chromosome segregation defects. *Mol. Biol. Cell* **14**, 3821-3833.

Clouthier, D. E., Hosoda, K., Richardson, J. A., Williams, S. C., Yanagisawa, H., Kuwaki, T., Kumada, M., Hammer, R. E. and Yanagisawa, M. (1998). Cranial and cardiac neural crest defects in endothelin-A receptor-deficient mice. *Development* **125**, 813-824.

de la Cruz, M. V., Sanchez-Gomez, C. and Palomino, M. A. (1989). The primitive cardiac regions in the straight tube heart (Stage 9$^-$) and their anatomical expression in the mature heart: an experimental study in the chick embryo. *J. Anat.* **165**, 121-131.

Delorme, B., Dahl, E., Jarry-Guichard, T., Briand, J. P., Willecke, K., Gros, D. and Theveniau-Ruissy, M. (1997). Expression pattern of connexin gene products at the early developmental stages of the mouse cardiovascular system. *Circ. Res.* **81**, 423-437.

Eckardt, D., Kirchhoff, S., Kim, J. S., Degen, J., Theis, M., Ott, T., Wiesmann, F., Doevendans, P. A., Lamers, W. H., de Bakker, J. M. et al. (2006). Cardiomyocyte-restricted deletion of connexin43 during mouse development. *J. Mol. Cell. Cardiol.* **41**, 963-971.

Galli, D., Dominguez, J. N., Zaffran, S., Munk, A., Brown, N. A. and Buckingham, M. E. (2008). Atrial myocardium derives from the posterior region of the second heart field, which acquires left-right identity as Pitx2c is expressed. *Development* **135**, 1157-1167.

Georges, R., Nemer, G., Morin, M., Lefebvre, C. and Nemer, M. (2008). Distinct expression and function of alternatively spliced Tbx5 isoforms in cell growth and differentiation. *Mol. Cell. Biol.* **28**, 4052-4067.

Goetz, S. C., Brown, D. D. and Conlon, F. L. (2006). TBX5 is required for embryonic cardiac cell cycle progression. *Development* **133**, 2575-2584.

Hoogaars, W. M., Barnett, P., Moorman, A. F. and Christoffels, V. M. (2007). T-box factors determine cardiac design. *Cell. Mol. Life Sci.* **64**, 646-660.

Ishii, Y., Fukuda, K., Saiga, H., Matsushita, S. and Yasugi, S. (1997). Early specification of intestinal epithelium in the chicken embryo: a study on the localization and regulation of CdxA expression. *Dev. Growth Differ.* **39**, 643-653.

Jiang, X., Rowitch, D. H., Soriano, P., McMahon, A. P. and Sucov, H. M. (2000). Fate of the mammalian cardiac neural crest. *Development* **127**, 1607-1616.

Kanegae, Y., Lee, G., Sato, Y., Tanaka, M., Nakai, M., Sakaki, T., Sugano, S. and Saito, I. (1995). Efficient gene activation in mammalian cells by using recombinant adenovirus expressing site-specific Cre recombinase. *Nucleic Acids Res.* **23**, 3816-3821.

Kedzierski, R. M., Grayburn, P. A., Kisanuki, Y. Y., Williams, C. S., Hammer, R. E., Richardson, J. A., Schneider, M. D. and Yanagisawa, M. (2003). Cardiomyocyte-specific endothelin A receptor knockout mice have normal cardiac function and an unaltered hypertrophic response to angiotensin II and isoproterenol. *Mol. Cell. Biol.* **23**, 8226-8232.

Kelly, R. G., Brown, N. A. and Buckingham, M. E. (2001). The arterial pole of the mouse heart forms from Fgf10-expressing cells in pharyngeal mesoderm. *Dev. Cell* **1**, 435-440.

Kirby, M. (2007). *Cardiac Development*. New York: Oxford University Press.

Koibuchi, N. and Chin, M. T. (2007). CHF1/Hey2 plays a pivotal role in left ventricular maturation through suppression of ectopic atrial gene expression. *Circ. Res.* **100**, 850-855.

Kokubo, H., Tomita-Miyagawa, S., Hamada, Y. and Saga, Y. (2007). Hesr1 and Hesr2 regulate atrioventricular boundary formation in the developing heart through the repression of Tbx2. *Development* **134**, 747-755.

Kurihara, Y., Kurihara, H., Suzuki, H., Kodama, T., Maemura, K., Nagai, R., Oda, H., Kuwaki, T., Cao, W. H., Kamada, N. et al. (1994). Elevated blood pressure and craniofacial abnormalities in mice deficient in endothelin-1. *Nature* **368**, 703-710.

Kurihara, Y., Kurihara, H., Oda, H., Maemura, K., Nagai, R., Ishikawa, T. and Yazaki, Y. (1995). Aortic arch malformations and ventricular septal defect in mice deficient in endothelin-1. *J. Clin. Invest.* **96**, 293-300.

Laugwitz, K. L., Moretti, A., Caron, L., Nakano, A. and Chien, K. R. (2008). Islet1 cardiovascular progenitors: a single source for heart lineages? *Development* **135**, 193-205.

Maemura, K., Kurihara, H., Kurihara, Y., Oda, H., Ishikawa, T., Copeland, N. G., Gilbert, D. J., Jenkins, N. A. and Yazaki, Y. (1996). Sequence analysis, chromosomal location, and developmental expression of the mouse preproendothelin-1 gene. *Genomics* **31**, 177-184.

Meilhac, S. M., Esner, M., Kelly, R. G., Nicolas, J. F. and Buckingham, M. E. (2004). The clonal origin of myocardial cells in different regions of the embryonic mouse heart. *Dev. Cell* **6**, 685-698.

Mjaatvedt, C. H., Nakaoka, T., Moreno-Rodriguez, R., Norris, R. A., Kern, M. J., Eisenberg, C. A., Turner, D. and Markwald, R. R. (2001). The outflow tract of the heart is recruited from a novel heart-forming field. *Dev. Biol.* **238**, 97-109.

Moorman, A. F. and Christoffels, V. M. (2003). Cardiac chamber formation: development, genes, and evolution. *Physiol. Rev.* **83**, 1223-1267.

Nagy, A., Gertsenstein, M., Vintersten, K. and Behringer, R. (2003). *Manipulating the Mouse Embryo: a Laboratory Manual*, 3rd edn. Cold Spring Harbor, NY: Cold Spring Harbor Laboratory Press.

Niu, Z., Yu, W., Zhang, S. X., Barron, M., Belaguli, N. S., Schneider, M. D., Parmacek, M., Nordheim, A. and Schwartz, R. J. (2005). Conditional mutagenesis of the murine serum response factor gene blocks cardiogenesis and the transcription of downstream gene targets. *J. Biol. Chem.* **280**, 32531-32538.

Offermanns, S., Zhao, L. P., Gohla, A., Sarosi, I., Simon, M. I. and Wilkie, T. M. (1998). Embryonic cardiomyocyte hypoplasia and craniofacial defects in G alpha q/G alpha 11-mutant mice. *EMBO J.* **17**, 4304-4312.

Ozeki, H., Kurihara, Y., Tonami, K., Watatani, S. and Kurihara, H. (2004). Endothelin-1 regulates the dorsoventral branchial arch patterning in mice. *Mech. Dev.* **121**, 387-395.

Prall, O. W., Menon, M. K., Solloway, M. J., Watanabe, Y., Zaffran, S., Bajolle, F., Biben, C., McBride, J. J., Robertson, B. R., Chaulet, H. et al. (2007). An Nkx2-5/Bmp2/Smad1 negative feedback loop controls heart progenitor specification and proliferation. *Cell* **128**, 947-959.

Sato, T., Kawamura, Y., Asai, R., Amano, T., Uchijima, Y., Dettlaff-Swiercz, D. A., Offermanns, S., Kurihara, Y. and Kurihara, H. (2008a). Recombinase-mediated cassette exchange reveals the selective use of Gq/G11-dependent and -independent endothelin 1/endothelin type A receptor signaling in pharyngeal arch development. *Development* **135**, 755-765.

Sato, T., Kurihara, Y., Asai, R., Kawamura, Y., Tonami, K., Uchijima, Y., Heude, E., Ekker, M., Levi, G. and Kurihara, H. (2008b). An endothelin-1 switch specifies maxillomandibular identity. *Proc. Natl. Acad. Sci. USA* **105**, 18806-18811.

Schaart, G., Viebahn, C., Langmann, W. and Ramaekers, F. (1989). Desmin and titin expression in early postimplantation mouse embryos. *Development* **107**, 585-596.

Srivastava, D., Cserjesi, P. and Olson, E. N. (1995). A subclass of bHLH proteins required for cardiac morphogenesis. *Science* **270**, 1995-1999.

Sugden, P. H. (2003). An overview of endothelin signaling in the cardiac myocyte. *J. Mol. Cell. Cardiol.* **35**, 871-886.

Takeuchi, J. K., Ohgi, M., Koshiba-Takeuchi, K., Shiratori, H., Sakaki, I., Ogura, K., Saijoh, Y. and Ogura, T. (2003). Tbx5 specifies the left/right ventricles and ventricular septum position during cardiogenesis. *Development* **130**, 5953-5964.

van den Berg, G., Abu-Issa, R., de Boer, B. A., Hutson, M. R., de Boer, P. A., Soufan, A. T., Ruijter, J. M., Kirby, M. L., van den Hoff, M. J. and Moorman, A. F. (2009). A caudal proliferating growth center contributes to both poles of the forming heart tube. *Circ. Res.* **104**, 179-188.

Waldo, K. L., Kumiski, D. H., Wallis, K. T., Stadt, H. A., Hutson, M. R., Platt, D. H. and Kirby, M. L. (2001). Conotruncal myocardium arises from a secondary heart field. *Development* **128**, 3179-3188.

Wilkinson, D. (1992). *In Situ Hybridization: a Practical Approach*. Oxford, UK: IRL Press.

Yamada, M., Revelli, J. P., Eichele, G., Barron, M. and Schwartz, R. J. (2000). Expression of chick Tbx-2, Tbx-3, and Tbx-5 genes during early heart development: evidence for BMP2 induction of Tbx2. *Dev. Biol.* **228**, 95-105.

Yanagisawa, H., Hammer, R. E., Richardson, J. A., Williams, S. C., Clouthier, D. E. and Yanagisawa, M. (1998). Role of Endothelin-1/Endothelin-A receptor-mediated signaling pathway in the aortic arch patterning in mice. *J. Clin. Invest.* **102**, 22-33.

Yuan, S. and Schoenwolf, G. C. (2000). Islet-1 marks the early heart rudiments and is asymmetrically expressed during early rotation of the foregut in the chick embryo. *Anat. Rec.* **260**, 204-207.

Zhou, B., Ma, Q., Rajagopal, S., Wu, S. M., Domian, I., Rivera-Feliciano, J., Jiang, D., von Gise, A., Ikeda, S., Chien, K. R. et al. (2008). Epicardial progenitors contribute to the cardiomyocyte lineage in the developing heart. *Nature* **454**, 109-113.

RESEARCH ARTICLE

Establishment of Mice Expressing EGFP in the Placode-Derived Inner Ear Sensory Cell Lineage and FACS-Array Analysis Focused on the Regional Specificity of the Otocyst

Chisato Fujimoto,[1,2] Hidenori Ozeki,[1,2] Yasunobu Uchijima,[1] Keigo Suzukawa,[2] Akihisa Mitani,[1,3] Shigetomo Fukuhara,[4] Koichi Nishiyama,[1] Yukiko Kurihara,[1] Kenji Kondo,[2] Hiroyuki Aburatani,[5] Kimitaka Kaga,[2] Tatsuya Yamasoba,[2] and Hiroki Kurihara[1]*

[1]Department of Physiological Chemistry and Metabolism, Graduate School of Medicine, The University of Tokyo, Bunkyo-ku, Tokyo, 113-0033, Japan
[2]Department of Otolaryngology, Graduate School of Medicine, The University of Tokyo, Bunkyo-ku, Tokyo, 113-8655, Japan
[3]Department of Respiratory Medicine, Graduate School of Medicine, The University of Tokyo, Bunkyo-ku, Tokyo, 113-8655, Japan
[4]Department of Structural Analysis, National Cardiovascular Center Research Institute, Suita, Osaka, 565-8565, Japan
[5]Genome Science Division, Research Center for Advanced Science and Technology, The University of Tokyo, Meguro-ku, Tokyo, 153-8904, Japan

ABSTRACT

In this study, we established a novel enhanced green fluorescent protein (EGFP) reporter mouse line that enables the visualization of the placode-derived inner ear sensory cell lineage. EGFP was initially expressed in the otic placode and throughout its differentiation process into the inner ear sensory patches. At embryonic day 10.5 (E10.5), EGFP was expressed in the ventral and dorsomedial region of the otocyst. These regions could mainly give rise to the cochlea, including the organ of Corti, and the saccule, including the macula and the endolymphatic duct. The region could also give rise to cells that will develop as either prosensory cells or statoacoustic ganglion neuroblasts. By using this line and fluorescence-activated cell sorting (FACS)-array technology, we developed a new gene expression profile of the regional specificity of the otocyst. EGFP-positive regions include the *Otx1*-positive region, which could be clearly distinguished from EGFP-negative regions. The signal log ratio of microarray data showed high efficiency in predicting the genes expressed mainly in the ventral and/or dorsomedial otocyst and the data could be mined to uncover many novel genes involved in inner ear morphogenesis and cell fate regulation. Additionally, these data suggest that some novel genes enriched in EGFP-positive regions may be potentially involved in human congenital sensorineural hearing loss. This reporter line could play important roles in the use of animal models for detailed analysis of the differentiation process into the sensory patches and the identification of regional-specific gene networks and novel gene functions in the developing inner ear. J. Comp. Neurol. 518:4702–4722, 2010.

INDEXING TERMS: transgenic mice; green fluorescent protein; inner ear; fluorescence-activated cell sorting; gene expression profiling; receiver operating characteristic

The inner ear of vertebrates is a complex sensory structure that derives from ectodermal thickenings of the head called otic placodes (Kaufman and Bard, 1999; Kiernan et al., 2002). The acquisition of inner ear axial identity from surrounding tissues probably begins after otic placode formation and involves early cell fate decisions (Bok et al., 2007). These early cell fate decisions can be classified into neural-fated cells, prosensory cells, and nonsensory epithelial cells. Neural-fated cells delaminate from the otic epithelium to form neurons of the statoacoustic

Additional Supporting Information may be found in the online version of this article.

Grant sponsor: the Global COE Program (Integrative Life Science Based on the Study of Biosignaling Mechanisms) (MEXT), the Ministry of Education, Culture, Sports, Science, and Technology Japan; Grant number: 21390238; Grant sponsor: the Ministry of Health, Labor, and Welfare of Japan; Grant number: H21-Seibutsushigen-Ippan-001.

*CORRESPONDENCE TO: Hiroki Kurihara, Department of Physiological Chemistry and Metabolism, Graduate School of Medicine, The University of Tokyo, 7-3-1, Hongo, Bunkyo-ku, Tokyo 113-0033, Japan.
E-mail: kuri-tky@umin.ac.jp

Received February 11, 2010; Revised June 2, 2010; Accepted July 1, 2010
DOI 10.1002/cne.22468
Published online July 26, 2010 in Wiley Online Library (wileyonlinelibrary.com)

ganglion (SAG) (Carney and Silver, 1983; Rubel and Fritzsch, 2002). Prosensory cells differentiate into mechanosensory hair cells and nonsensory supporting cells (Kelley et al., 1995; Fekete et al., 1998). The sense of hearing and equilibrium in vertebrates are controlled by epithelial sensory patches in the cochlea and vestibule of the inner ear and their dominant neurons. Many genes induced within the otic epithelium as a result of axial specificity continue to mediate inner ear morphogenesis, such as the interaction between prosensory and nonsensory epithelial cells (Bok et al., 2007). Elucidating the signals providing axial specificity, the resultant molecular events from existing signals, and the regional-specific genes related to neural/sensory organ formation is important in understanding inner ear morphogenesis.

One major approach to clarify the novel molecular mechanism of the morphogenesis is to reliably profile the spatiotemporal expression of genes within this complex organ. Several microarray expression profiling studies of the murine inner ear have been reported (Chen and Corey, 2002; Liu et al., 2004; Powles et al., 2004; Morris et al., 2005; Sajan et al., 2007). Although these studies may contribute to identifying and analyzing expressed genes, more powerful tools for dissecting genetically, morphologically, and/or regionally defined cell populations for transcriptome analysis are required. The combination of the green fluorescent protein (GFP) reporter strain and the fluorescence-activated cell sorting (FACS) system has allowed sampling of purified cell populations (Lobo et al., 2006; Marsh et al., 2008). To date, none of these approaches have been attempted during the developmental stage of the inner ear.

GFP reporter mice have been widely used for the imaging of biologically important cell populations. For analysis of the developing inner ear, previous studies have used some reporter lines in which GFP expression is driven by promoters of the sine oculis related homeobox 1 homolog (*Drosophila*) (*Six1*) (Ozaki et al., 2004) and the mouse homolog of the *Drosophila* atonal gene (*Math1*) (Lumpkin et al., 2003). For example, *Six1*-expressing cells were detected by GFP luminescence in heterozygous embryos from the otic placode to the nonsensory area of the cochlea (Ozaki et al., 2004). After division into vestibular and auditory compartments, the *Math1*-GFP reporter system can be a powerful tool to monitor the differentiation of the prosensory precursors to hair cells (Lumpkin et al., 2003). However, to our knowledge, there are no lines for spatiotemporally monitoring the cell lineage from the otic placode to both sensory and neural cell differentiation.

In the present study, we established transgenic mouse lines in which enhanced GFP (EGFP) expression was driven by the promoter of endothelin receptor type A gene (*Ednra*). One of the lines exhibited ectopic EGFP expression in the developing inner ear. EGFP expression was initially detected in the otic placode and throughout its differentiation into the inner ear sensory patches. This line has unprecedented significance as a reporter system to monitor the placode-derived sensory cell lineage during inner ear development. We focused on the E10.5 stage, when EGFP expression of the transgenic line was detected mainly in the ventral and dorsomedial regions of the otocyst. The otocyst undergoes a sequence of further evaginations and tissue remodelings to form the embryonic inner ear, which is divided into vestibular and auditory compartments. At this stage, transcription could be active in the already existing signals related to axial specificity and in regionally specific genes including genes related to neural/sensory organ formation. We sorted the otocyst epithelial cells into EGFP-positive and EGFP-negative cells, profiled the expression of the genes in FACS-enriched cell population, and conducted transcriptome analysis. The use of this novel transgenic line and FACS-array technology in the present study provides an insight into a comprehensive understanding of the molecular mechanisms underlying organogenesis and cell fate regulation in the inner ear.

MATERIALS AND METHODS

Construction of Ednra-EGFP transgenic mice

The *Ednra-EGFP* transgene used for generation of transgenic mice was constructed as follows. The *EGFP* coding sequence flanked by *Eco*RI and *Xho*I restriction sites (~0.7 kb) was generated from the pIRES2-EGFP vector (Clontech, Palo Alto, CA) by polymerase chain reaction (PCR) with 5′-GAATTCAACCATGGTGAGCAAG-3′ (forward primer) and 5′-CTCGAGTTACTTGTACAGCTCG-3′ (reverse primer). The EGFP coding sequence was subsequently ligated into the pCEFL-HA vector (Murga et al., 1998) via the *Eco*RI-*Xho*I restriction site to yield the *EGFP*-pCEFL-HA vector. A polyadenylation signal from bovine growth hormone (BGHpA) was located downstream of the EGFP coding sequence in the *EGFP*-pCEFL-HA vector.

The *Ednra* sequence, containing the promoter region and exon1 of the mouse *Ednra* gene, flanked by *Eco*RI restriction sites, was generated by genomic PCR with 5′-GAATTCTTTCTCTCTGAATATTTAAC-3′ (forward primer) and 5′-CTTAAGAGCTCCTCGGAAGCAGACA-3′ (reverse primer). The *Ednra* sequence was ligated into the *EGFP*-pCEFL-HA vector to construct a ~ 3.2-kb *Ednra-EGFP*-BGHpA sequence. A *Ednra-EGFP*-BGHpA fragment obtained by restriction digestion with the *Eco*RI and *Pvu*II enzymes was excised from the pCEFL-HA vector, purified, and injected into fertilized eggs with C57BL/6 genetic backgrounds. Founder animals were identified by Southern blot analysis by using an *EGFP*-specific ^{32}P-labeled

probe, and progenies were routinely detected by PCR with transgene-specific oligonucleotides (data not shown). We have established several *Ednra-EGFP* transgenic mouse lines with the *Ednra-EGFP* transgene. One line, named *Tg(ETAR-EGFP)14Imeg* (hereafter termed Line-14), exhibited ectopic EGFP expression in the developing inner ear. Another line, named *Tg(ETAR-EGFP)1Imeg* (hereafter termed Line-1), exhibited no ectopic expression in the ear and served as the control in genomic analysis.

All procedures were carried out in accordance with the University of Tokyo Animal Care Protocols and the National Institutes of Health *Guide for the Care and Use of Laboratory Animals*.

Southern blot analysis

Genomic DNA was extracted from a part of the tails of the mice by the standard technique and digested with an appropriate restriction enzyme, electrophoresed in a 0.8% agarose gel, transferred to a Nytran SuPerCharge membrane (Schleicher & Schuell Bioscience, Keene, NH), and hybridized with the EGFP portion of the transgene radiolabeled with [^{32}P]deoxycytidine triphosphate. Then 657 bp of the EGFP sequence, which was used as the template to synthesize the radiolabeled probe, was generated by PCR with 5′-AGCTGGACGGCGACGTAAAC-3′ (forward primer) and 5″-CTCGTCCATGCCGAGAGTGA-3′ (reverse primer). The probe was constructed by using Megaprime DNA labeling systems (Amersham Biosciences, Piscataway, NJ). Membranes were washed under high stringency conditions and autoradiographs were obtained.

Colony PCR-based screening

Line-14 genomic DNA fragments digested with *Eco*RI were electrophoresed in an agarose gel, and ~2.8-kb fragments were dissected from the gel and purified by using Wizard SV Gel and PCR Clean-Up System (Promega, Madison, WI) following the manufacturer's instructions. The fragments were ligated into the vector pCRII-TOPO (Invitrogen, Carlsbad, CA) according to the manufacturer's instructions. The resulting construct was transformed to DH5-alpha by 37°C heat shock. The transformation solution in SOC medium was plated on an appropriate LB-agar/ampicillin (100 μg/ml) plate and incubated overnight at 37°C. Colonies picked from the plate were used as templates for PCR amplification. The above-mentioned EGFP-specific primers were used for colony PCR. We selected clones that possessed the EGFP sequence, and the construct was then sequenced.

Genome walking method

To identify the integrated regions of the transgene, libraries were constructed by using the GenomeWalker Universal Kit (Clontech, Mountain View, CA). Homozygous Line-14 and wild-type genomic DNA were digested separately with four restriction enzymes–*Eco*RV, *Dra*I, *Pvu*II, and *Stu*I. Digested DNA was purified according to the manufacturer's protocol. A GenomeWalker adaptor was ligated to both ends of the digested, purified DNA. Gene-specific primers were designed within the promoter region of the *Ednra* gene (gsp1 5′-GGATTGTCAGGG GTGCTGAGAGGCAAA-3′; gsp2 5′-ACTCCTGACTACTGAG GCAACAGCAGT-3″, and the BGHpA region (gsp1 5′-GAG GATTGGGAAGACAATAGCAGGCA-3′; gsp2 5′-GGATGCG GTGGGCTCTATGGCTTCTGA-3a′). The primary PCR reaction was carried out with the AP1 adaptor and gsp1 primers; subsequent nested PCR was carried out with the AP2 adaptor and gsp2 primers. The PCR cycling conditions were established according to the manufacturer's protocol. Amplification was performed on a GeneAmp PCR System 9700 (Applied Biosystems, Foster City, CA). Products were visualized on a 1.5% agarose gel and gel-purified by using Wizard SV Gel and PCR Clean-Up System (Promega) according to the manufacturer's instructions. Products were directly sequenced without cloning.

Auditory and vestibular function tests

The vestibular function of mice was assessed with the swim test (Khan et al., 2004). Normal mice could swim with their heads above water for the entire 60 seconds; however, mice with vestibular dysfunction could keep their heads above water for no more than a few seconds (Khan et al., 2004). Here, 2-month-old mice were placed in a cage filled with water at room temperature for 60 seconds. The average swimming time with the head above water was determined for three trials for each mouse.

The auditory function of mice was evaluated by their auditory brainstem response (ABR) at 2 months of age. ABR is an evoked potential measurement of auditory activity of the cochlea, auditory nerve, and central auditory pathway in the brainstem. It is often used as a technique in auditory research in humans and laboratory animals (Pourbakht and Yamasoba, 2003). Homozygous and heterozygous 2-month-old *Ednra-EGFP* Line-14 transgenic mice and wild-type controls were anesthetized with a mixture of xylazine hydrochloride (10 mg/kg, i.m.) and ketamine hydrochloride (40 mg/kg, i.m.). Before the ABR test, the tympanic membranes or tympanic cavities were confirmed to be normal in all mice. When the paw pinch reflex disappeared, three electrodes were placed subcutaneously on the vertex of the head (active electrode), in the

TABLE 1.
Primary Antibodies Used in Immunohistochemistry

Antigen	Immunogen	Manufacturer	Dilution
Green Flourescent Protein (GFP)	Full length amino acid sequence derived from *Aequorea victoria*.	Abacam (Cambridge, MA, USA), goat polyclonal, ab6673	1:100
Myosin 7a (Myo7a)	Amino acids 880-1077 from the tail region of human myosin 7a.	Proteus Biosciences (Ramona, CA, USA), rabbit polyclonal, 25-6790	1:100
P^{27kip1}	Amino acids 175-198 derived from c-terminal of human P^{27kip1}.	Thermo Fisher Scientific (Fremont, CA, USA), rabbit polyclonal, RB-9019	1:100
SRY-box containing gene 2 (Sox2)	Synthetic peptide (sequence, SSSPPVVTSSSHSRAPC) from human Sox2. The immunogen sequence iis dentical in human and mouse.	Chemicon (Temecula, CA, USA), rabbit polyclonal, AB5603	1:1000

postauricular region of the measured ear (reference electrode), and in the postauricular region of the opposite ear (ground). The speaker was located 10 cm from the tragus of the stimulated ear. A tone burst stimulus (2, 4, 8, 16, and 32 kHz) was produced by using a sound stimulator (Neuropack Σ MEB-5504; Nihon Kohden, Tokyo, Japan). The duration of the stimulus was 15 milliseconds, the presentation rate was 11/second, and the rise/fall time was 1 millisecond. At each intensity level (5-dB steps) to assess the threshold, the ABR was determined by averaging 500 responses. The threshold was visually defined as the lowest intensity level at which a clear reproducible waveform was visible in the trace. An overall test for differences among homozygous Line-14 mice, heterozygous Line-14 mice, and wild-type controls was performed for each frequency by using one-way analysis of variance (ANOVA) ($P < 0.05$). Statistical analyses were conducted by using SPSS version 11.0J (SPSS Japan, Tokyo, Japan).

Antibody characterization

All antibodies used in this study are listed in Table 1. The GFP antibody recognized the expected (27-kDa) band on a Western blot of GFP-positive transgenic rat aorta and showed no cross-reactivity with the rat endogenous arterial proteins mentioned in a previous report (Rodriguez-Menocal et al., 2009). In the present study, the antibody stained the inner ear in Line-14 EGFP-positive transgenic mice but not in wild-type mice (Fig. 1). The myosin 7a (*Myo7a*) antibody displayed the classic hair cell-specific labeling distribution (Hasson et al., 1995; Bermingham-McDonogh et al., 2006) and exhibited similar labeling in a variety of species including the mouse (Hasson et al., 1997). The $p27^{kip1}$ antibody recognized the expected (27-kDa) band on a Western blot of murine neonatal organ of Corti (Chen and Segil, 1999). $p27^{kip1}$ immunohistochemistry showed staining in the primordial organ of Corti and differentiated supporting cells of the mature organ of Corti (Chen and Segil, 1999). The appropriate controls of the SRY- box containing gene 2 (*Sox2*) antibody for Western blotting are mouse or human embryonic stem cell lysate and mouse embryonic germ cell lysate (manufacturer's datasheet). The antibody recognized a 34-kDa band corresponding to *Sox2* on Western blots of whole cell or nuclear extracts; this band was not observed in cytosolic extracts. The antibody stained tissue in wild-type mice but not in conditional *Sox2*-knockout mice (Favaro et al., 2009).

Histological and immunohistochemical analyses

The tissues of adult mice were fixed by cardiac perfusion with ice-cold 4% paraformaldehyde (PFA) in phosphate-buffered saline (PBS; pH 7.4) followed by decapitation. Mouse embryos were fixed in 4% PFA in PBS. For adults, the heads were fixed in 4% PFA in PBS and decalcified in 10% ethylenediamine tetraacetic acid for several days. Then the specimens were dehydrated in ethanol series and embedded in paraffin. The paraffin block containing the tissue was cut into 4-μm sections. The sections were deparaffinized and then rehydrated through xylene and ethanol series. For hematoxylin-eosin staining, the sections were stained with Carrazi's hematoxylin (Muto Pure Chemicals, Tokyo, Japan), treated with 1% HCl in 70% ethanol for differentiation, stained in eosin solution (1% Eosin Y [Merck, Darmstadt, Germany]:80% ethanol/glacial acetic acid = 100:375:1 [v/v/v]), dehydrated, and mounted.

For immunohistochemical staining, the sections were placed in citrate-buffered solution (pH 6.0; Dako Cytomation Japan, Kyoto, Japan) and autoclaved at 121°C for 20 minutes for antigen retrieval. Sections were incubated for 1 hour with a blocking solution (PBS [pH 7.4] containing 5% skim milk [Wako, Osaka, Japan], 0.1% Triton-X 100, and 0.1% sodium azide) at room temperature to reduce nonspecific antibody binding. The sections were then incubated with primary antibody overnight at 4°C in the blocking solution.. The secondary antibodies used were Alexa Fluor 488 donkey anti-goat IgG (Invitrogen; 1:200